Rahman, M.M.; Filiz, V.; Shishatskiy, S.; Abetz, C.; Neumann, S.; Bolmer, S.; Khan, M.M.; Abetz, V.:

PEBAX® with PEG functionalized POSS as nanocomposite membranes for CO2 separation

In: Journal of Membrane Science (2013) Elsevier

DOI: 10.1016/j.memsci.2013.03.001

PEBAX® with PEG functionalized POSS as nanocomposite membranes for CO_2 separation

Md. Mushfequr Rahman, Volkan Filiz*, Sergey Shishatskiy, Clarissa Abetz, Silvio Neumann, Sabrina Bolmer, Muntazim Munir Khan, Volker Abetz*

Helmholtz-Zentrum Geesthacht, Institute of Polymer Research, Max-Planck-Straße 1, 21502 Geesthacht, Germany

Corresponding E-Mail : volkan.filiz@hzg.de, volker.abetz@hzg.de
Tel. +49 4152 872461

Abstract

Nanocomposite membranes were prepared by incorporation of commercial poly(ethylene glycol) functionalized polyoctahedral oligomeric silsesquioxanes (PEG-POSS) in two grades of poly(ether-*block*-amide) namely PEBAX® MH 1657 and PEBAX® 2533. Single gas permeabilities of N_2, O_2, CH_4, H_2, and CO_2 were measured using the time-lag method. CO_2 permeability increased two fold after incorporation of 30 wt% PEG-POSS in PEBAX® MH 1657, while the selectivity was not significantly affected at 30 °C. Simultaneous enhancement in permeability and selectivity was observed up to 30 wt% loading of PEG-POSS in PEBAX® 2533 at 30 °C. The effect of temperature upon CO_2 permeability and CO_2 selectivity over N_2, O_2, CH_4 and H_2 was studied between 30 ºC to 70 °C. Substantial influence upon the thermal transition of the polyether domain of both polymers was observed due to incorporation of PEG-POSS by differential scanning calorimetry (DSC). Atomic force microscopy was used to evaluate the impact of 30 wt% PEG-POSS loading upon the surface topography of both investigated grades of PEBAX®. Scanning electron microscopy (SEM) and energy

dispersive X-ray spectroscopy (EDS) were used to study the membrane morphology and the distribution of the nanofillers (PEG-POSS) in PEBAX® membranes.

Keywords

Nanocomposite membrane, PEBAX® membrane, PEG-POSS, CO_2 separation.

1. Introduction

Polymer based gas separation membranes have already emerged as a realistic platform for use in large scale industries, serving as competitive candidates for traditional thermally driven separation processes. [1] However, a major drawback of polymer based membranes has been the naturally counteracting permeability and selectivity. The development of new membrane materials with improved permeability, selectivity and stability is required to overcome this drawback in order to improve the process efficiency for industrial applications. Incorporation of inorganic particles is a promising alternative approach to overcome the limitations of regular polymer membrane. In this approach, both porous and non-porous inorganic fillers are used as dispersed phase in polymer matrices. Porous fillers act as molecular sieving agents in the polymer matrix and selectively allow the desired component to pass through the pores, when the polymer chains wet the porous particles completely and there are no defects. [2] Conventional speculation was that incorporation of nonporous or impermeable fillers in a polymer membrane will lead to a systematic reduction of permeability due to increased tortuosity of the diffusion path as well as reduced solubility of the separating gas molecules in the polymer matrix. Different models have been proposed to describe this phenomenon. One of the most widely used models is the Maxwell Model. However, it has been reported in many studies that incorporation of impermeable nanofillers does not lad to a behavior following the Maxwell Model

and therefore can be an attractive choice to increase the permeability and selectivity of polymer based membranes. Interactions of the polymer matrix as well as the separating gas molecules with the surface of the impermeable nanofillers play a major role in the gas separation property of the nanocomposite membranes. [3-9]

In recent years, incorporation of nanosized macromer POSS (polyoctahedral oligomeric silsesquioxanes) into a polymer matrix has received considerable attention. POSS molecules have a rigid cage-like structure which is intermediate between silica and siloxane. The empirical formula can be rendered as $(RSiO_{1.5})_n$, n = 6 - 12, where R is various types of functional groups. A small particle (molecule) size in the range of 1 - 3 nm and the possibility of tailoring properties by introduction of various functional groups makes POSS an attractive candidate for organic inorganic hybrid nanocomposites. [10]

Commercially available thermoplastic elastomers poly(ether-*block*-amide) under the trade name PEBAX® having flexible polyether and rigid polyamide segments are known to be excellent materials for separation of CO_2 from light gases (e.g. H_2 or N_2). In these polymers the crystalline polyamide domains provide mechanical strength and act as intermediate spacers between the polyether domains hindering their crystallization and offering greater chain mobility of the ether linkage. The favorable interaction of polar ether oxygen with CO_2 results in high solubility selectivity of CO_2 over non polar gases. [11, 12] Studies have been reported to increase the permeability of a hydrophilic grade PEBAX® MH 1657 (60 wt% poly(ethylene oxide) and 40 % polyamide 6) without affecting the selectivity by incorporation of low molecular weight polyethers. Higher permeability appears to stem from the increase in polyether content of the membrane, as well as increase in total free volume. [13, 14] Moreover, a low molecular weight copolymer containing 20 wt% of polydimethylsiloxane as a backbone and 80 wt% of poly(ethylene glycol) (PEG) as a side chain was reported to increase the permeability even more than pure PEG. [15] Recently, molecular level mixed matrix membranes comprising PEBAX® and POSS

have been reported to exhibit simultaneous enhancement in CO_2 permeability and CO_2/H_2 selectivity at extremely low POSS loadings. [16]

The motivation of this work is to study the effect of incorporation of a commercial nano particle PEG-POSS (poly(ethylene glycol) modified polyoctahedral oligomeric silsesquioxanes) upon the gas transport properties and to gain insight into the thermal properties as well as surface topography of two different grades of PEBAX®.

2. Materials

Two grades of commercial PEBAX namely, PEBAX® MH 1657 and PEBAX® 2533 were purchased from ARKEMA. PEG-POSS was purchased from Hybrid Plastics®. The solvents- ethanol (99.9 wt%) and *n*-butanol (99.5 wt%) were purchased from Merck KGaA and Scharlau Chemie S. A. respectively. All these chemicals were used as received.

3. Methods

3.1. Preparation of Nanocomposites

Dense membranes were prepared by solution casting in Teflon molds. Mixtures of PEG-POSS and PEBAX® MH 1657 were dissolved in a mixture of ethanol/water (70/30 wt%) under reflux (80 °C) for 2 h. Similarly, mixtures of PEG-POSS and PEBAX® 2533 were

dissolved in *n*-butanol at 70 °C for 2 h. The concentration of the solution was 3 wt% and the PEG-POSS content was varied from 10-50 wt% of the polymer. After cooling to room temperature the obtained homogeneous solution was filtered through a 32 μm stainless steel filter and poured into Teflon molds. The solutions of PEBAX® MH 1657 and PEG-POSS were dried for 24 hours, while those of PEBAX® 2533 and PEG-POSS were dried for 48 h at 40 °C. The films were dried under vacuum overnight at 30 °C. Membrane thickness was measured by a digital micrometer and they varied from 100 to 200 μm.

3.2. Characterization

Single gas permeability of the prepared dense membranes was determined by the constant volume, variable pressure ("time lag") method within the temperature range 30 ºC to 70 ºC. The order of the gases was N_2, O_2, CH_4, H_2, CO_2, N_2 and the feed pressure was 1 bar for all the gases. Each measurement was repeated 3 times and for each polymer-POSS composition 3 membrane samples were measured.

Differential scanning calorimetry (DSC) was used to study the effect of incorporation of nanoparticles upon thermal transition of both the grades of PEBAX® in the temperature range from -100 ºC to 250 ºC. All DSC runs were performed in a DSC 1 (Star system) from Mettler Toledo using a nitrogen purge gas stream (60 mL/min) at a scan rate of 10 K/min. Heating and cooling scans were performed by initially heating the sample up to 100 ºC and holding it at that temperature for 5 minutes in order to erase the effects resulting from any previous thermal history, then the sample was cooled down to -100 ºC. Finally a second heating scan up to 250 ºC and a second cooling scan down to -100 ºC were applied. The DSC thermograms presented here correspond to the second heating and second cooling.

Atomic force microscope (AFM) images were taken on a Multimode AFM (NanoScope® IVa Controller) from Veeco (now Bruker) operating in tapping mode at room temperature using commercial silicon AFM tips (model MPP 11100) with a free resonance frequency in the range from 268 to 333 kHz and spring constants in the range from 20 to 80 N/m.

The scanning electron microscope (Merlin, Zeiss) equipped with an EDS system (Oxford) was used to characterize both surface and cross section morphology of the samples with secondary electrons (SE) and X-rays. The secondary electron images of the sample surface were taken at an accelerating voltage of 800V. The X-ray spectra were recorded at 3kV while the elemental mappings were performed at 5kV. To avoid charging effects of the non-conducting polymer using accelerating voltages of 3 and 5kV the samples were coated with a very thin layer of Pt. The spatial resolution of the EDS analysis is in the range of approx. 0.5-1 µm, therefore homogeneity of the elemental maps (here we focus on Si, C, O) can only be discussed on this length scale.

4. Results

4.1. Chemical Structure and composition

Table 1: Composition of two grades of PEBAX®.

The compositions of PEBAX® polymers used for this study are summarized in Table 1. [11-13] POSS used as nanofiller for this study (the structure available from manufacturer is presented in Figure 1(a)) is functionalized with poly(ethylene glycol) which has the same chemical structure as that of the amorphous phase of PEBAX® MH 1657. But in the other case (i.e PEBAX® 2533) the amorphous phase is composed of a different polyether, namely poly(tetramethylene oxide).

Figure 1: Composition of PEG-POSS (a) Structure provided by manufacturer (b) Thermogravimetric analysis.

From the structure and molecular weight provided by the supplier, the weight percentage of poly(ethylene glycol) surrounding the POSS was calculated. According to the calculation PEG-POSS consists of approx. 92 wt% poly(ethylene glycol). Thermogravimetric analysis (TGA) of PEG-POSS is presented in Figure 1(b). In TGA 88 % mass loss was observed between 100 – 700 ºC and 11.5 % residue was left at 995 ºC, which is in accordance with the calculation made from the structure. The mass loss reveals that the commercial PEG-POSS is decorated with more than 88 wt% poly(ethylene glycol) which degraded between 100 – 700 ºC and the residual mass comes from the cage structure of oligomeric silsesquioxanes as well as some carbonaceous residues. Hence, the commercial PEG-POSS contains higher weight percentage of polyether than both PEBAX® MH 1657 and PEBAX® 2533 which means incorporation of PEG-POSS increases the total polyether content of the nanocomposite prepared by both the grades of PEBAX® significantly.

4.2. Gas Separation Performance

Gas permeability (P), diffusion coefficient (D), solubility (S) and ideal selectivity of membranes for pure gases ($\alpha_{A/B}$) were obtained from time-lag measurements using the following equations-

$$P = D.S = \frac{V_p.l}{A.R.T.\Delta t} \ln \frac{p_f - p_{p1}}{p_f - p_{p2}} \quad (1)$$

$$D = \frac{l^2}{6\theta} \quad (2)$$

$$\alpha_{A/B} = \frac{P_A}{P_B} \quad (3)$$

where, V_p is the permeate volume, l is the membrane thickness, A is the membrane area, R is the gas constant, Δt is the time difference between two points (1 and 2) on the pressure curve, p_f is the feed pressure considered constant in the time range Δt, p_{p1} and p_{p2} are permeate pressures at time moment 1 and 2, and θ is the time lag, respectively. The temperature dependence of P, D and S within the range where no thermal transition occurs is described as (Arrhenius relationship) –

$$P = P_o \exp^{\frac{-E_P}{RT}} \quad (4)$$

$$D = D_o \exp^{\frac{-E_D}{RT}} \quad (5)$$

$$S = S_o \exp^{\frac{-\Delta H_S}{RT}} \quad (6)$$

Here, P_o, D_o and S_o are pre-exponential constants, E_P is the activation energy of permeation, E_D is the activation energy of diffusion and ΔH_S is the enthalpy of sorption. From equation 1, 4 and 5 the following relationship can be obtained-

$$E_P = E_D + \Delta H_S \quad (7)$$

The last 3 parameters are related according to the solution-diffusion model. [17]

Figure 2: Single gas permeability as a function of PEG-POSS content in PEBAX® MH1657. Permeability of N_2, O_2, CH_4 and H_2 are plotted on left Y axis and that of CO_2 right Y axis.

Figure 2 shows the values of single gas permeabilities of pure PEBAX® MH 1657 and the composites prepared by incorporation of PEG-POSS as a function of PEG-POSS content. Significant increase in permeability of all the gases was observed up to 30 wt% PEG-POSS incorporation. The permeability of CO_2 increased from 73 to 152 barrer, this means that the permeability of a nanocomposite membrane containing 30 wt% PEG-POSS was two times higher than of pure PEBAX® MH 1657. For higher amounts of PEG-POSS (40 wt% and 50 wt%) the membranes became too soft to be fixed in the measurement cell of the time lag measurement facility.

Figure 3: CO_2 selectivity over light gases as a function of PEG-POSS content in PEBAX® MH1657.

Figure 3 clearly shows that, due to 10 % incorporation of PEG-POSS the selectivity of the membrane decreased slightly but as the PEG-POSS content was increased to 20 and 30 wt%, similar selectivity like PEBAX® MH 1657 was found for all four gas pairs. The loss of selectivity at 10 wt% PEG-POSS loading, in spite of increase in total polyether content may be related with the crystallinity of the polyether domain (discussed in detail in section 4.3).

Figure 4: Diffusion coefficient and solubility of CO_2 as a function of PEG-POSS content in PEBAX® MH1657.

To gain insight into the effect of PEG-POSS incorporation upon the gas transport mechanism through the membrane, diffusion coefficient and solubility of CO_2 are plotted as a function of PEG-POSS content in Figure 4. It was observed that at a loading with

10 wt% PEG-POSS the diffusion coefficient was slightly lower than for pure PEBAX® MH 1657. However, as the error bars overlap each other, the decrease in diffusion of CO_2 in the membrane is actually not significant. But at higher loadings of PEG-POSS a significant increase of the diffusion coefficient was observed. The solubility of CO_2 appeared to increase with increasing of PEG-POSS content. It is already well established that, ethylene oxide units provide very good solubility of condensable CO_2 gas in the polymer membrane due to affinity of the polar ether oxygen and quadrapolar CO_2 gas. [18] Hence, the solubility of CO_2 is directly related with the increase of ether oxygen in the nanocomposite membrane.

Figure 5: Single gas permeability as a function of PEG-POSS content in PEBAX® 2533. Permeability of N_2, O_2, CH_4 and H_2 are plotted on left Y axis and that of CO_2 right Y axis.

Incorporation of PEG-POSS in PEBAX® 2533 also increased the permeability of the membranes up to 30 wt% loading, as represented in Figure 5. But, the increase in permeability was not as significant as in case of PEBAX® MH 1657. 30 wt% PEG-POSS loading in PEBAX® 2533 leads to 32 % higher permeability of CO_2 than that of pure PEBAX® 2533. For higher PEG-POSS content, permeability of the gases showed a decreasing trend and after incorporation of 50 wt% PEG-POSS the permeability of the gases through the nanocomposite membrane was well below the permeability through the pure polymer membrane, although the ether oxygen content is higher in 50 wt% PEG-POSS containing nanocomposite membrane than that of pure PEBAX® 2533.

Figure 6: CO_2 selectivity over light gases as a function of PEG-POSS content in PEBAX® 2533.

In contrast to what was observed in the case of PEBAX® MH 1657, incorporation of PEG-POSS leads to an increase in selectivity of the membrane in PEBAX® 2533, as evident from Figure 6. The selectivities of CO_2/N_2, CO_2/O_2, CO_2/CH_4 and CO_2/H_2 of the pure PEBAX® 2533 were found to be 26, 10, 8, and 5, respectively, while those of PEBAX® 2533 with 50 wt% PEG-POSS nanocomposite membrane increased to 35, 14, 10, and 6, respectively.

Figure 7: Diffusion coefficient and solubility of CO_2 as a function of PEG-POSS content in PEBAX® MH1657.

From Figure 7 it is also clear that an incorporation of PEG-POSS into PEBAX® 2533 has a different impact upon the gas transport mechanism through the membrane compared to that in PEBAX® MH 1657. In this case diffusion of CO_2 remains unchanged upto incorporation of 30wt % PEG-POSS and at higher loadings it drops significantly. However, the solubility of CO_2 increases significantly with the increase of PEG-POSS content what is similar to what was observed for PEBAX® MH 1657. These observations elucidate the fact that at PEG-POSS loadings higher than 30 wt% the permeability of CO_2 shows a decreasing trend (Figure 5) because of the significant drop of diffusion through the membrane (Figure 7). The steady increase of CO_2 selectivity for all four gas pairs (Figure 6), with the incorporation of PEG-POSS content stems from the increase of CO_2 solubility (Figure 7) in the membrane.

Figure 8: Permeability of gases as a function of temperature of PEBAX® MH1657 and PEBAX® 2533 before and after 30 wt% PEG-POSS incorporation.

Since at 30 °C the best gas separation performance was observed for 30 wt% PEG-POSS loading in both grades of PEBAX®, this composition was chosen to study the effect of temperature upon CO_2 separation. Figure 8 shows that permeability of all the gases increases with increasing temperature in pure PEBAX® as well as in PEG-POSS containing nanocomposite membranes. But a careful examination reveals that, although the nanocomposite membrane prepared from PEBAX® 2533 has a higher permeability of CO_2 and similar permeability of other gases (N_2, O_2, CH_4 and H_2) at relatively low temperatures (e.g. 30 °C and 40 ºC), the increase of gas permeability with the increase of temperature for the nanocomposite membrane is not as significant as that of the pure polymer membrane. Especially, the permeability of H_2 is considerably lower in the nanocomposite membrane at 70 °C. On the other hand, in PEBAX® MH 1657 the permeability of all the gases is higher in the nanocomposite membrane than in the pure polymer membrane at all temperatures.

.

Figure 9: CO_2 selectivity over light gases as a function of temperature of PEBAX® MH1657 and PEBAX® 2533 before and after incorporation of 30 wt% PEG-POSS.

Polyether based membranes are notorious for loss of CO_2 selectivity over light gases with the increase of temperature. Figure 9 shows that both grades of PEBAX® have lost CO_2 selectivity significantly for all four gas pairs with the increase of temperature with and without incorporation of 30 wt% PEG-POSS. Hence, incorporation of PEG-POSS did not prevent the loss of CO_2 selectivity at high temperature. However, the selectivity of CO_2 over H_2 of PEG-POSS containing PEBAX® 2533 nanocomposite membrane was found to be slightly higher than the pure polymer membrane up to 50 °C.

Figure 10: Diffusion coefficient and solubility of CO_2 as a function of temperature of PEBAX® MH1657 and PEBAX® 2533 before and after 30 wt% PEG-POSS incorporation.

Figure 10 shows that for all four membranes diffusion of CO_2 increases substantially while solubility of CO_2 undergoes a dramatic decrease with the increase of temperature. Interestingly, it was observed that diffusion of CO_2 increased much more significantly with the increase of temperature in the PEBAX® 2533 membrane than the corresponding nanocomposite membrane. However, for PEBAX® MH 1657, the diffusion coefficient seemed to have slightly higher value at all temperatures after PEG-POSS incorporation.

Table 2: E_P, E_D and ΔH_S of PEBAX® MH1657 and PEBAX® 2533 before and after 30 wt% PEG-POSS incorporation.

E_P calculated from the slope of *ln P* vs *1000/T* (using equation 4), E_D calculated from the slope of *ln D* vs *1000/T* (using equation 5) and ΔH_S calculated from equation 7 are plotted in Table 2. A positive value of E_P is attributed to the increase of permeability with the increase of temperature. A significant drop of E_P can be noticed in PEG-POSS incorporated nanocomposite membranes compared to the pure polymer membrane. Therefore, the rate of increase of CO_2 permeability as a function of temperature is lower in the nanocomposite membranes compared to the pure polymer membrane (although CO_2 permeability is higher at all temperatures within 30 °C to 70 °C for the PEG-POSS containing PEBAX® MH 1657 nanocomposite membrane). For PEBAX® 2533 the drop of E_P of CO_2 was more significant (around 36 %) than that of PEBAX® MH 1657 (around 20 %). Comparing the values of E_D and ΔH_S it is clear that, change of both E_D and ΔH_S of CO_2 contributed to the observed change of E_P. E_D corresponds to the energy required for a penetrant to make a diffusive jump from one equilibrium sight to another. Lower values of E_D of CO_2 in the nanocomposite membranes is a result of lower rate of increase of CO_2 diffusion as a function of temperature after 30 wt% PEG-POSS incorporation in both the grades of PEBAX®. As in the case of PEBAX® 2533 incorporation of 30 wt% PEG-POSS led to a drop of both diffusion

coefficient as a function of temperature and E_D of CO_2; it can be assumed that the degree of freedom involved in the diffusion process is less in the nanocomposite membrane. [19, 20] A negative value of ΔH_S is the characteristic for decrease of sorption with increase of temperature which is in accordance with the loss of solubility observed in Figure 10. A more negative ΔH_S value or higher change of enthalpy in the nanocomposites compared to the pure polymer elucidates the fact that PEG-POSS provided a favorable sorption environment for the polar CO_2 due to the increase of polar ether oxygen content in both grades of PEBAX®. As the polyether segments of PEBAX® 2533 are composed of the relatively less polar repeating unit (tetramethylene oxide), the incorporation of PEG-POSS, containing more polar repeating units of the functional group (ethylene oxide), makes a more significant contribution to this behavior in this polymer compared with PEBAX® MH 1657.

4.3. Thermal Analysis

Table 3: Glass transition temperature of PEBAX® MH1657 and PEBAX® 2533 as a function of PEG-POSS content.

In Table 3 the effect of PEG-POSS content upon glass transition temperature (T_g) obtained from DSC is shown. The T_gs that correspond to the polyether blocks were observable in all the samples, while the T_gs for polyamide blocks were impossible to detect by DSC. But the melting points of both polyether and polyamide blocks are visible. It was observed that the glass transition temperature of PEBAX® 2533 was significantly lower than that of PEBAX® MH 1657. T_gs gradually decreased with the increase of PEG-POSS content in PEBAX® MH 1657 upto 30 wt% and for higher PEG-POSS content T_g was not clearly observable. However, in the case of PEBAX® 2533 no substantial influence was observed upon the glass transition temperature due to incorporation of PEG-POSS. Hence, PEG-POSS acts as a plasticizer for PEBAX® MH 1657 but not for PEBAX® 2533.

Figure 11: DSC thermograms (second heating trace) of PEBAX® MH1657 and its nanocomposites with PEG-POSS.

Figure 11 shows the effect of PEG-POSS content in PEBAX® MH1657 content upon the melting of polyether and polyamide domains (second heating cycle of DSC thermogram). In pure PEBAX® MH1657 two characteristic melting endotherms were observed, which is consistent with the microphase separated structure of the block copolymer. [12] The melting endotherm observed with an onset, peak and endset temperature of 2.3 ºC, 18.1 ºC and 25.4 ºC, respectively, is attributed to the melting of the polyether domains and proves its molten nature at 30.0ºC (gas permeability was measured within 30ºC to 70 ºC). The other melting endotherm with an onset temperature 190.1 ºC, peak temperature 203.7 ºC and endset temperature 21 ºC comes from the melting of the polyamide domains. The thermal transition of the polyamide blocks does not seem to be affected by the incorporation of PEG-POSS, as the onset, peak and endset temperature was not significantly influenced after addition of PEG-POSS. On the other hand, significant changes were observed on the melting of the polyether domains due to incorporation of PEG-POSS. With the increase of PEG-POSS content the onset temperature of the melting endotherm shifted to -0.6, -3.5, - 9.1, - 16.1 and -16.9 ºC, respectively. At 40 and 50 wt% loading a small shoulder is visible at lower temperature in the melting endotherm. This phenomenon reveals the fact that the polyether of PEG-POSS starts to melt at a lower temperature than that of PEBAX® MH1657, indicating that it might not be homogeneously mixed into the polyether domains at these higher loadings.

Figure-12: DSC thermogram (second cooling trace) of PEBAX® MH1657 and its nanocomposites with PEG-POSS.

The cooling scan of pure PEBAX® MH1657 in Figure 12 shows that crystallization of polyamide block starts at 166 °C upon cooling from the melt and as the temperature is decreased further, crystallization of the polyether blocks starts at -12°C. The onset, peak and endset temperatures of the crystallizing exotherms attributed to the polyether domains as a function of PEG-POSS content are summarised in Table 4.

Table 4: Onset, peak and endset temperature of crystallization of polyether domain of PEBAX® MH1657 as a function of PEG-POSS content.

It was observed that the crystallization exotherm of polyether domains shifted to higher temperature due to incorporation of PEG-POSS upto 20 wt%, i.e. the crystallization of polyether blocks occurred at a higher temperature while cooling down from the melt after incorporation of PEG-POSS. This observation elucidates the fact that PEG-POSS acts as a nucleating agent on the polyether domain of this type of PEBAX. However, for higher loading (30, 40 and 50 wt%) of PEG-POSS, no further shift was observed.

Figure 13: DSC thermogram (second heating trace) of PEBAX® 2533 and its nanocomposites with PEG-POSS.

The heating cycles of DSC thermograms representing the effect of PEG-POSS content in PEBAX® 2533 upon melting are plotted in Figure13. To discuss the multiple melting endotherms in this figure the peaks are designated as I, II, III and so on with the increase of their position on the temperature scale. The endothermic peak observed between -14 °C to 34 °C having the maximum at 12.7 °C (peak III) for pure PEBAX® 2533 is attributed to the melting of the polyether domains. Two adjacent melting endotherms (peak IV and V) observed above 100ºC come from the melting of the polyamide domains. The endothermic transition (peak IV) prior to the main melting peak (peak V) refers to the existence of secondary crystallization phenomenon inside the polyamide phase. Peak IV

might be attributed to the melting of poorly small polyamide crystals. [21, 22] Even after incorporation of PEG-POSS both peaks IV and V were visible at the same temperatures and the shape remained unchanged. On the other hand, significant changes were observed on the melting of the polyether domains due to incorporation of PEG-POSS. At 10 wt% loading a small new peak (peak II) appears at lower temperature. With the increase of PEG-POSS content peak II becomes bigger, but its position in the temperature scale remains constant. Although peak III becomes smaller with the increase of PEG-POSS content, it is clearly distinguishable from peak II even after 50 wt% PEG-POSS loading. This phenomenon reveals the fact that; the ether of PEG-POSS melts at a lower temperature than the ether of PEBAX which is in accordance with PEBAX® MH 1657 observed in Figure 6. However, after 20wt% loading another endothermic peak (peak I) starts to appear and becomes non-negligible at 30, 40 and 50 wt% loading. This refers to the PEG ligands of PEG-POSS, as it also was observed for the PEBAX® MH 1657 nanocomposite membrane.

Figure 14: DSC thermogram (second cooling trace) of PEBAX® 2533 and its nanocomposites with PEG-POSS.

Figure 14 shows the effect of PEG-POSS content in PEBAX® 2533 upon the cooling cycle of DSC thermogram. Upon cooling from the melt, the major portion of polyamide starts to crystallize just below 105.0 ºC, while a small fraction of polyamide can only crystallize at much lower temperature (below 55 ºC). No change of the shape or position in the temperature scale of polyamide peaks was observed after incorporation of PEG-POSS. The crystallization peak for polyether domains was -12.3ºC for pure PEBAX® 2533 and it shifted to -12.4 ºC, -14.3 ºC, -13.4 ºC, -17.2 ºC and -16.3 ºC with the increase of PEG-POSS content upto 50 wt%. However, at 40 and 50 wt% loading multiple peaks were observed and it is clearly visible from the position of the multiple peaks at the temperature scale that a part of the polyether domains crystallizes exactly at the same temperature as pure PEBAX® 2533. The appearance of multiple peaks both at heating and cooling traces leads to the hypothesis that at higher PEG-POSS loadings a fraction of PEG-POSS may be ejected from the polyether domains of PEBAX® 2533 and exist as aggregates.

4.4. Surface Topography

The surface topography of the films was characterized by AFM. Nevertheless, only 30 wt% PEG-POSS incorporated nanocomposite membranes were compared with the pure PEBAX® of both grades to study the effect of incorporation of nanoparticles upon the surface roughness.

Figure-15: Surface topography via AFM a) 3D- image of PEBAX® MH1657 c) 3D-image of 30 wt% PEG-POSS incorporated PEBAX® MH1657 b) Height image of PEBAX® MH1657 d) Height image of 30 wt% PEG-POSS incorporated PEBAX® MH1657.

The 3D images obtained by AFM from a sample area of 10 μm x 10 μm are presented in Figure 15 (a) and (c) for PEBAX® MH1657 and PEBAX® MH1657 with 30 wt% PEG-POSS, respectively. The 3D images reveal the presence of nanoscale roughness on the surface of both pure PEBAX® MH1657 and the nanocomposite membrane. It is evident from the 3D images that no clusters or agglomerates appeared on the surface of the nanocomposite membrane even for this rather high level of loading with PEG-POSS. This shows the compatibility of the nanoparticles with the polymer matrix. The height images corresponding to Figure 15 (a) and (c) are presented in Figure 15 (b) and (d), which show that the nanocomposite samples have more bright and dark spots which correspond to the highest and lowest points of the surface. Moreover, the maximum vertical distance between the highest and lowest point for pure PEBAX® MH1657 is 182 nm than that of the nanocomposite sample which is 304 nm. The roughness parameters are listed in

Table 5 where R_{max}, R_q and R_a represent the maximum height, route mean square deviation of height, and the average deviation of height respectively. Hence, it is evident that in the case of the nanocomposite membrane with 30 wt% PEG-POSS nanoparticles the surface roughness is higher which might have occurred due to surface reorganization of the polymer chains due to the presence of nanoparticles.

Table 5: Roughness parameters of PEBAX® MH1657 and its nanocomposite after incorporation of 30 wt% PEG-POSS.

Figure 16: Surface topography via AFM a) 3D- image of PEBAX® 2533 c) 3D-image of 30 wt% PEG-POSS incorporated PEBAX® 2533 b) Height image of PEBAX® 2533 d) Height image of 30 wt% PEG-POSS incorporated PEBAX® 2533.

In contrary to PEBAX® MH1657, no nanoscale roughness was observed in PEBAX® 2533. From the 3D and corresponding height images (Figure 16 (a) and 16 (b)) it is visible that the roughness present on the surface of PEBAX® 2533 is on a micrometer scale. Figure 16 (c) shows that after incorporation of PEG-POSS the surface topography has changed and the roughness disappeared across a large part of the surface. Meanwhile some irregular nanoscale bumps were observed on the surface of the membrane of PEBAX® 2533 with 30 wt% PEG-POSS. The roughness calculation of these images is presented in Table 6. Hence, although some new nanoscale roughness appeared, the overall surface became smoother after incorporation of PEG-POSS compared to that of pure PEBAX® 2533. These results indicate that the distribution of the nanofillers is different in the two types of PEBAX® and therefore further investigations were carried out by scanning electron microscopy.

Table 6: Roughness parameters of PEBAX® 2533 and its nanocomposite after incorporation of 30 wt% PEG-POSS.

4.5. SEM and EDS analysis

Figure 17: Surface morphology and surface spectra of PEBAX® nanocomposite membranes containing 30 wt% PEG-POSS. a) SEM micrograph of PEBAX® MH1657 nanocomposite membrane; b) SEM micrograph of PEBAX® 2533 nanocomposite membrane; c) EDS spectra of two areas of PEBAX® MH1657 nanocomposite membrane; d) EDS spectra of two areas of PEBAX® 2533 nanocomposite membrane.

The surface morphology and also the EDS spectra of representative areas are shown in Figure 17 for nanocomposite membranes of PEBAX® MH 1657 (Figure 17 a, c) and PEBAX® 2533 (Figure 17 b, d), respectively. Both nanocomposite membranes contain 30 wt% PEG-POSS. For the PEBAX® MH 1657 nanocomposite membrane the surface revealed a needle like structure which is due to the crystalline polyamide (Polyamide 6) part of the polymer. The regions in between these needles correspond to the polyether blocks i.e. the poly(ethylene oxide) blocks, which contribute 60 wt% to the multiblock copolymer. The lateral segregation of these two domains is too small to reveal the selective localisation of PEG-POSS in the polyether microdomains. However, DSC results shown in section 4.3 indicate that polyamide blocks melt at the same temperature in the nanocomposite membrane as it does in pure PEBAX® MH 1657. Therefore the EDS spectra presented in Figure 17 c show a homogeneous distribution of PEG-POSS all over the surface (or surface near regions) within the polyether domains of the mutiblock copolymer. Hence, it is evident that the PEG-ligands of the PEG-

POSS nanofiller introduced miscibility with the polyether domains of the multiblock copolymer PEBAX® MH 1657. In contrast, the surface of the PEBAX® 2533 nanocomposite membrane showed distinct darker regions with a needlelike structure and other, smoother regions appeared bright. The needlelike structure corresponds to polyamide (Polyamide 12) blocks, the crystalline component contributing 20 wt% to this multiblock copolymer, while the smoother areas correspond to locations, where the amorphous Poly(tetramethylene oxide) blocks cover the surface. In this sample rich and poor regions of PEG-POSS are clearly distinguishable from the comparison of the characteristic X-ray peaks for Si and O of the spectra recorded in a bright and dark region, respectively (Figure 17 d). The strong appearance of Na is probably due to impurities. Another important issue is the distribution of PEG-POSS all over the thickness of the membranes. The cross-sectional morphologies of these two samples are shown in Figures 18 and 19. Figure 18 shows a homogeneous morphology of the PEBAX® MH 1657 nanocomposite membrane, while Figure 19 shows an inhomogeneous structure with ellipsoidal inclusions for the PEBAX® 2533 nanocomposite membrane. These inclusions are located all over the cross section of the membrane, and they are larger and more numerous versus the top of the membrane. They are a result of the poor miscibility of PEG-POSS with the poly(tetramethylene oxide) domains, what will become more evident from the elemental mapping figures shown in Figure 21.

Figure 18: SEM micrograph of the cross section of a PEBAX® MH1657 nanocomposite membrane containing 30 wt% PEG-POSS.

Figure 19: SEM micrograph of the cross section of a PEBAX® 2533 nanocomposite membrane containing 30 wt% PEG-POSS

Figure 20: Cross section morphology of a PEBAX® MH1657 nanocomposite membrane containing 30 wt% PEG-POSS a) SEM micrograph b) Si element map c) C element map d) O element map

Figure 21: Cross section morphology of a PEBAX® 2533 nanocomposite membrane containing 30 wt% PEG-POSS a) SEM micrograph b) Si element map c) C element map d) O element map

Figures 20a-d show a section of the cross sectional morphology of the PEBAX® MH 1657 nanocomposite membrane, and the corresponding elemental mappings of C, Si and O, respectively. These images show that the nanofillers are homogeneously distributed within the sample, at least on the length scale of spatial resolution of the EDS analysis. The analogous investigation for the PEBAX® 2533 nanocomposite membrane is shown in Figure 21. The elemental maps reveal two clearly separated areas of PEBAX® 2533 and PEG-POSS. Due to the incompatibility of the PEG-ligands with both components of this multiblock copolymer a macroscopic demixing is clearly seen, which is the reason for the occurance of the inclusions discussed before.

5. Discussion

5.1. Correlation between thermal and gas separation properties

It has been reported that blending low molecular PEG in PEBAX® MH1657 leads to a decrease in glass transition and melting temperature of the PEG domains and consequently the permeability of the membrane increases. [11, 12] A similar trend was observed after the incorporation of PEG- POSS into PEBAX® MH1657. In the case of PEBAX® 2533 the incorporation of PEG-POSS does not lead to a significant decrease of the glass transition temperature and the increase of gas permeability with the increase of PEG-POSS content at 30°C is also much less than in the case of PEBAX® MH1657 (section 4.3). The influence of the change in glass transition

temperature on the gas transport mechanism is clear from comparison of diffusion behaviour of CO_2 at 30 °C through both grades of PEBAX® nanocomposite membranes with loadings upto 30 wt% PEG-POSS (Figures 4 and 7). In the case of PEBAX® MH1657 the incorporation of PEG-POSS leads to a significant decrease of T_g or in other words it increased the flexibility of the polyether blocks. Consequently the diffusion of CO_2 also increases substantially after incorporation of 30 wt% PEG-POSS. On the other hand, PEG-POSS has no significant influence on the T_g of PEBAX® 2533 and the diffusion of CO_2 remains unchanged upto 30 wt% PEG-POSS loading. Since, PEG-POSS used for this study is decorated with low molecular weight poly(ethylene glycol) chains of the same chemical structure of polyether blocks of PEBAX® MH1657 and different from the polyether blocks of PEBAX® 2533 (section 4.1) it is expected that the compatibility of the PEG ligand of the nanoparticle with the polyether blocks of two different grades of PEBAX® is also different. Hence, a strong correlation between gas transport through the membrane and impact on the glass transition temperature due to different compatibility of the ligand of the nanoparticle with the polyether blocks of the block copolymer is evident. This argument seems to be further justified by the observation that incorporation of 30 wt% PEG-POSS into PEBAX® 2533 resulted in a lower diffusion of CO_2 at elevated temperature (e.g. 60 °C and 70 °C) while in the case of PEBAX® MH1657 it led to a higher diffusion of CO_2 within 30°C to 70 °C (Figure 10). Moreover, Figures 5 and 7 reveal the fact that at 40 and 50 wt % PEG-POSS loading in PEBAX® 2533 the permeability of CO_2 decreases dramatically at 30 °C due to decrease of diffusion through the nanocomposite membrane but the solubility shows an increasing trend. Meanwhile, DSC studies show multiple peaks during heating and cooling cycles at these compositions (section 4.3) and EDS analysis proved the existence of aggregates of PEG-POSS in PEBAX® 2533 (section 4.5). From all these observations it seems reasonable to assume that PEG-POSS did not plasticize the polyether blocks of PEBAX® 2533, rather it existed as agglomerates which provided favorable adsorption sites for polar CO_2 molecules but led to higher diffusion resistance (or hindered the diffusive jump from one site to another) due to the presence of a hypothetical interphase between the agglomerated nanoparticles and polymer matrix.

On the other hand, it was observed (section 4.5) that PEG-POSS is homogeneously dispersed in PEBAX® MH1657 and acts as a nucleating agent for the crystallization of the polyether domain (section 4.3). Since the polyether blocks of PEBAX® MH1657 have the same repeating unit as the ligand of PEG-POSS, it is expected that the rigid cage like structure of PEG-POSS will be wetted by the polymer chains completely which might facilitate the crystal formation in the polyether domains during the cooling from the melt. Hence, incorporation of PEG-POSS in PEBAX® MH1657 leads to two phenomena which counteract each other; increase of low molecular weight PEG content (which leads to plasticization or decrease of T_g) and too much compatibility of the ligand of the nanoparticle with the polymer segment (which leads to nucleation). Gases are virtually insoluble in the crystalline regions of the polymer when compared to amorphous rubbery regions. [23] However, it must also be considered that the single gas permeability of the membranes was measured between 30 ºC to 70 °C and the nucleation of the polyether domain by PEG-POSS was observed below 0 °C. Figure 6 shows the molten nature of the ether domain at 30 °C. Therefore, it is expected that the nucleating effect of PEG-POSS is irrelevant at any temperature in which gas transport measurements were carried out.

5.2. Correlation between surface topography and gas separation properties

Gas transport through dense polymeric membranes is believed to occur in three successive steps- sorption of the penetrant at the feed side of the membrane, diffusion of the penetrant through the membrane, and desorption at the permeate side. [24] The first step is likely to be related with available adsorption sites. The presence of roughness on the surface of the membrane provides more available adsorption sites than a completely smooth surface. In section 4.4 it was described that incorporation of 30 wt% PEG-POSS seemed to have increased the surface roughness of PEBAX® MH1657 and decreased that of PEBAX® 2533. Meanwhile, the increase of gas permeability of the membrane was also significantly lower in case of PEBAX® 2533 than PEBAX® MH1657 after incorporation of 30wt% PEG-POSS. For example, and increase of CO_2 permeability of ca. 100% was observed in PEBAX® MH1657 while in

PEBAX® 2533 it was only ca. 30%. In spite of the strong correlation between the change in glass transition temperature with increase of gas permeability (section 5.1), these observations suggest that increase of surface area which stems from the roughness of the surface might also have an impact on the gas transport through these membranes.

6. Conclusion

Commercial PEG-POSS is able to alter the gas separation performance of different grades of PEBAX® membranes significantly. The gas transport after incorporation of PEG-POSS is strongly related with the thermodynamic properties, while the surface roughness may also play a role. PEBAX® MH1657 with 30 wt% PEG-POSS showed substantial improvement in gas permeability without any significant change in selectivity within 30 °C to 70 °C. Hence, it can be concluded that PEG-POSS is a suitable nanofiller to improve the commercial viability of PEBAX® membranes containing poly(ethylene glycol) as a soft segment.

Acknowledgement

This work was financially supported by the 7th Framework Program research EU-project “HARCANA” (Grant Agreement No: NMP3-LA-2008-213277) and the Helmholtz Association of German Research Centres through the Helmholtz Portfolio MEM-BRAIN.

References

[1] W. J. Koros, Evolving beyond the thermal age of separation processes: Membranes can lead the way, AIChE J., 50 (2010) 2326-2334.

[2] M. A. Aroon, A. F. Ismail, T. Matsuura, M. M. Montazer-Rahmati, Performance studies of mixed matrix membranes for gas separation: A review, Sep. Purif. Technol., 75 (2010) 229-242.

[3] H. Cong, M. Radosz, B. F. Towler, Y. Shen, Polymer-inorganic nanocomposite membranes for gas separation, Sep. Purif. Technol., 55 (2007) 281-291.

[4] T. C. Merkel, B. D. Freeman, R. J. Spontak, Z. He, I. Pinnau, P. Meakin, A.J.Hill, Ultrapermeable Reverse-Selective nanocomposite membrane, Science, 296 (2002) 519.

[5] T. C. Merkel, B.D. Freeman, R. J. Spontak, Z. He, I. Pinnau, P. Meakin and A. J. Hill, Sorption, transport and structural evidence for enhanced free volume in poly(4-methyl-2-pentyne)/fumed silica nanocomposite membranes, Chem. Mater., 15 (2003) 109-123.

[6] T. C. Merkel, B.D. Freeman, R. J. Spontak, Z. He, I. Pinnau, P. Meakin and A. J. Hill, Effect of Nanoparticles on gas sorption and transport in Poly(1-trimethylsilyl-1-propyne) Macromolecules, 36 (2003), 6844–6855.

[7] T. C. Merkel, Z. He, I. Pinnau, Sorption and Transport in Poly(2,2-bis(trifluoromethyl)-4,5-difluoro-1,3-dioxole-co-tetrafluoroethylene) containing nanoscale fumed silica, Macromolecules, 36 (2003), 8406–8414.

[8] J. Ahn, W. J. Chung, I. Pinnau, M. D. Guiver, Polysulfone/ silica mixed-matrix membranes for gas separation, J. Membr. Sci., 314 (2008) 123-133.

[9] Y. Kong, H. Du, J. Yang, D. Shi, Y. Wang, Y. Zhang, W. Xin, Study on polyimide/TiO_2 nanocomposite membranes for gas separation, Desalination, 146 (2002) 49-55.

[10] B. S. R. Reedy, D. Gnanasekaran, Structure gas transport property relationship of poly(dimethyl siloxane-urethane) nanocomposite membranes, Advances in Nanocomposites – Synthesis, Characterization and Industrail Applications, 2011, InTech, ISBN 978-953-307-165-7, Ch 10, pp195-226 .

[11] V.I. Bondar, B. D. Freeman, I. Pinnau, Gas transport property of poly(ether-b-amide) segmented block copolymers, J. Polym. Sci., Part B: Polym. Phys., 38 (2000) 2051-2062.

[12] V.I. Bondar, B. D. Freeman, I. Pinnau, Gas Sorption and Characterization of poly(ether-b-amide) segmented block copolymers, J. Polym. Sci., Part B: Polym. Phys., 37 (1999) 2463-2475.

[13] A. Car, C. Stropnik, W. Yave, K. V. Peinemann, PEG modified poly(amide-*b*-ethyleneoxide) membranes for CO2 separation, J. Membr. Sci., 307 (2008) 88-95.

[14] W. Yave, A. Car, K. V. Peinemann, Nanostructurec membrane material designed for carbondioxide separation, J. Membr. Sci., 350 (2010) 124-129.

[15] S. R. Reijerkerk, M. H. Knoef, K. Nijmeijer, M. Wessling, Poly(ethylene glycol) and poly(dimethyl siloxane): Combining their advantages into efficient CO_2 gas separation membranes, J. Membr. Sci., 352 (2010) 126-135.

[16] Y. Li, T. S. Chung, Molecular-level mixed matrix membranes comprising PEBAX® and POSS for hydrogen purification via preferential CO_2 removal Int. J. Hydrogen Energy , 35 (2010) 10560-10568.

[17] S. Shishatskiy, J. R. Pauls, S. P. Nunes, K. V. Peinemann, Quaternary ammonium membrane materials for CO_2 separation, J. Membr. Sci. , 2010; 359(1–2):44–53.

[18] H. Lin, B. D. Freeman, Material selection guidelines for membranes that remove CO_2 from gas mixtures, J. Mol. Struct., 739 (2005) 57-74.

[19] T. K. Kwei, W. M. Arnheim, The diffusion of gases through filled polymers J. Polym. Sci.: Part C, (1965) 103-110.

[20] P. Meares, The diffusion of gases through polyvinyl acetate, J. Am. Chem. Soc., 76 (1954), 3415-3422.

[21] S. Fakirov, Poly(ether-*b*-amide) thermoplastic elastomers: Structure, properties and applications, Handbook of Condensation Thermoplastic Elastomer, 2005, WILEY-VCH Verlag GmbH & Co, ISBN 3-527-30976-4, ch-10, pp 263-267.

[22] S. T. Correale, N. S. Murthy, Secondary crystallization and premelting endo- and exotherms in oriented polymers, J. Appl. Polym. Sci., 101 (2006) 447-454.

[23] S. A. Stern, H. L. Frisch, The selective permeation of gases though polymers, Annu. Rev. Mater. Sci., 11 (1981) 523-550.

[24] E. R. Hensema, Polymeric gas separation membrane, Adv. Mater., 6 (1994) 269-279.

Tables and Figures

Table 1: Composition of two grades of PEBAX®.

Grade of PEBAX®	**Polyether Phase**	**Polyether Content (wt%)**	**Polyamide Phase**	**Polyamide Content (wt%)**
PEBAX® MH 1657	$-(CH_2-CH_2-O)_n-$ Poly(ethylene oxide)	60	$-(NH-(CH_2)_5-CO)_n-$ Polyamide 6	40
PEBAX® 2533	$-(CH_2-CH_2-CH_2-CH_2-O)_n-$ Poly(tetramethylene oxide)	80	$-(NH-(CH_2)_{11}-CO)_n-$ Polyamide 12	20

Table-2: E_P, E_D and ΔH_S of PEBAX® MH1657 and PEBAX® 2533 before and after 30 wt% PEG-POSS incorporation.

Composition	**E_p of CO_2 (kJ/mol)**	**E_D of CO_2 (kJ/mol)**	**ΔH_S of CO_2 (kJ/mol)**
PEBAX® 2533	16.7	27.2	-10.5
PEBAX® 2533 + 30 wt% PEG-POSS	10.3	22.2	-11.9
PEBAX® MH 1657	18.6	32	-13.4
PEBAX® MH 1657 + 30 wt% PEG-POSS	14.9	28.8	-13.9

Table 3: Glass transition temperature of PEBAX® MH1657 and PEBAX® 2533 as a function of PEG-POSS content.

PEG-POSS Content (wt%)	**Glass transition temperature (ºC)**	
	PEBAX® MH 1657	PEBAX® 2533
0	-52.0	-77.1
10	-52.9	-76.9
20	-53.6	-78.2
30	-57.8	-78.9
40	-	-78.2
50	-	-78.7

Table 4: Onset, peak and endset temperature of crystallization of polyether domain of PEBAX® MH1657 as a function of PEG-POSS content.

PEG-POSS Content (wt%)	**Crystallization exotherm of polyether domain**		
	Onset (°C)	Peak (ºC)	Endset (°C)
0	-12.3	-19.1	-27.5
10	-6.1	-14.3	-21.3
20	-4.6	-11.1	-18.7
30	-4.3	-10.5	-17.3
40	-4.3	-11.7	-16.8
50	-4.3	-10.7	-15.4

Table 5: Roughness parameters of PEBAX® MH1657 and its nanocomposite after incorporation of 30 wt% PEG-POSS.

Composition	**R_{max} (nm)**	**R_q (nm)**	**R_a (nm)**
PEBAX® MH1657	182	18.1	14
PEBAX® MH1657 + 30 wt% PEG-POSS	304	43.6	35

Table 6: Roughness parameters of PEBAX® 2533 and its nanocomposite after incorporation of 30 wt% PEG-POSS.

Composition	**R_{max} (nm)**	**R_q (nm)**	**R_a (nm)**
PEBAX® 2533	888	131	108
PEBAX® 2533 + 30 wt% PEG-POSS	224	39.7	32.7

Figure 1:

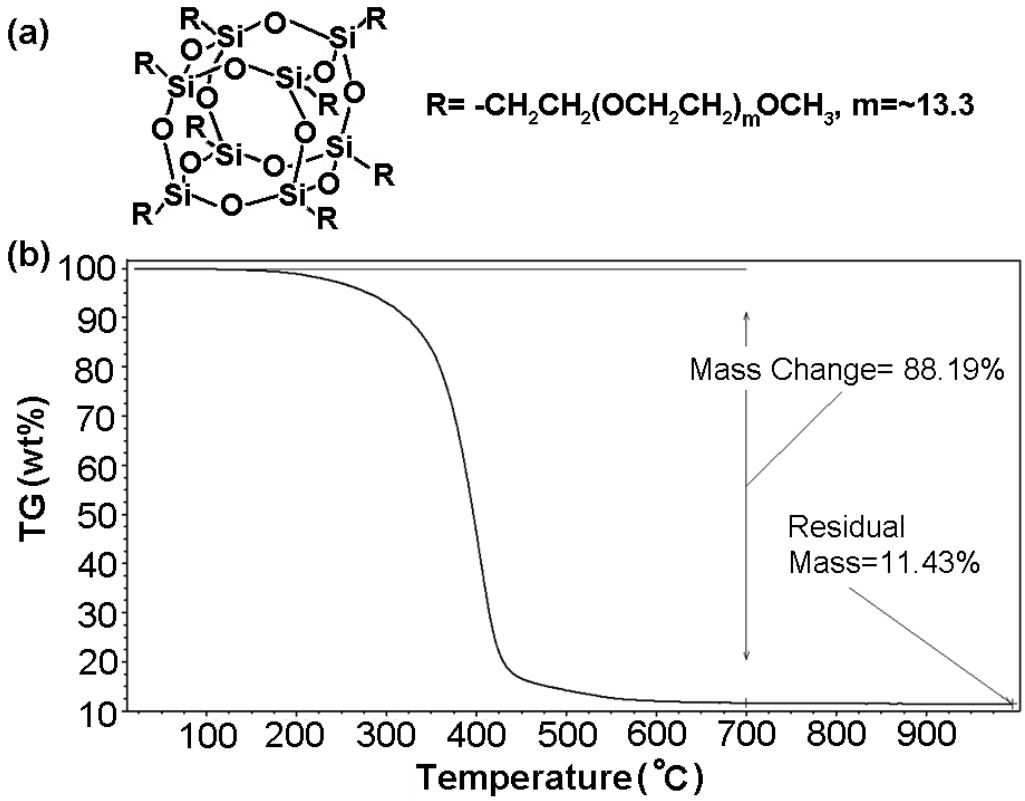
(a)
R= -CH2CH2(OCH2CH2)mOCH3, m=~13.3
(b)
TG (wt%)
100
90
80
70
60
50
40
30
20
10
100 200 300 400 500 600 700 800 900
Temperature(°C)
Mass Change= 88.19%
Residual
Mass=11.43%

Figure 2:

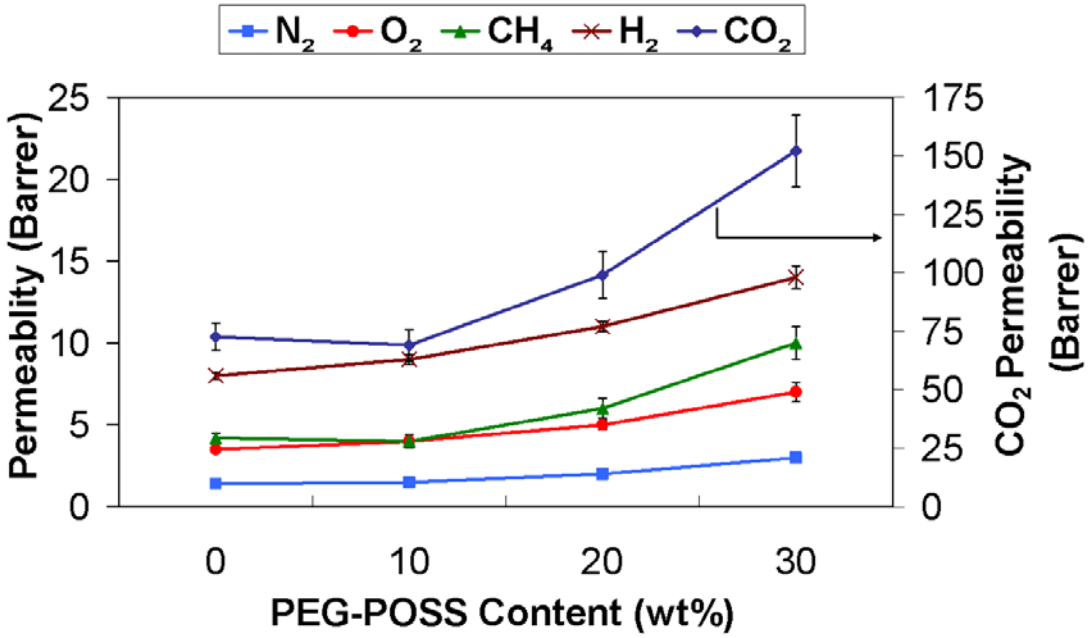
N2
O2
CH4
H2
CO2
Permeablity (Barrer)
CO2 Permeability (Barrer)
PEG-POSS Content (wt%)
0
5
10
15
20
25
0
25
50
75
100
125
150
175
0
10
20
30

Figure 3:

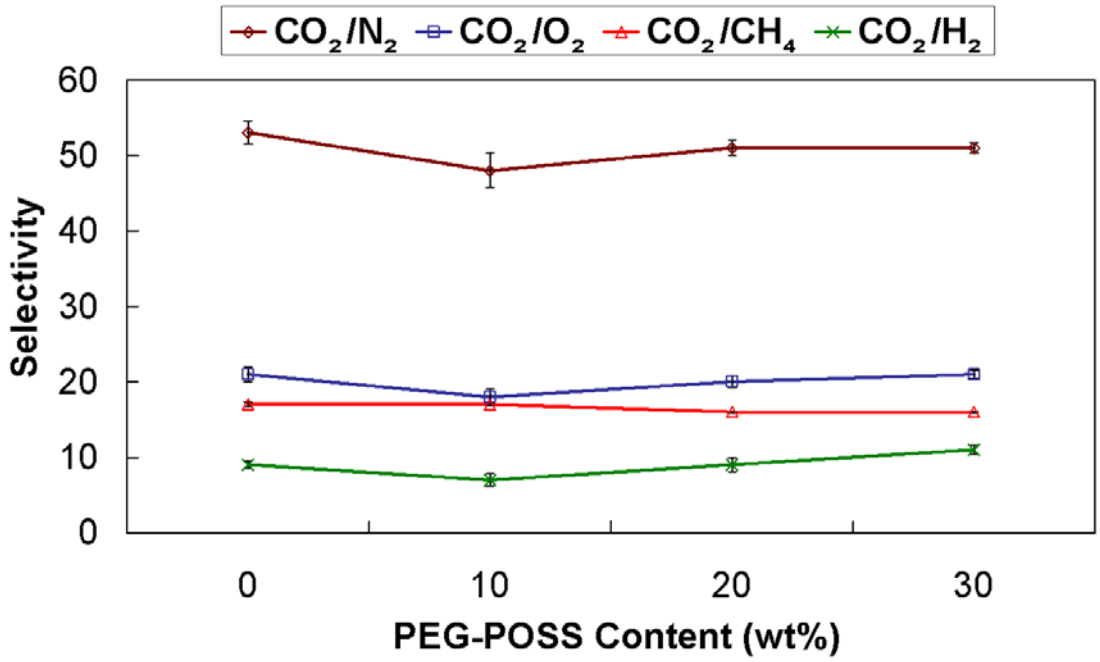
CO2/N2
CO2/O2
CO2/CH4
CO2/H2
Selectivity
60
50
40
30
20
10
0
0
10
20
30
PEG-POSS Content (wt%)

Figure 4:

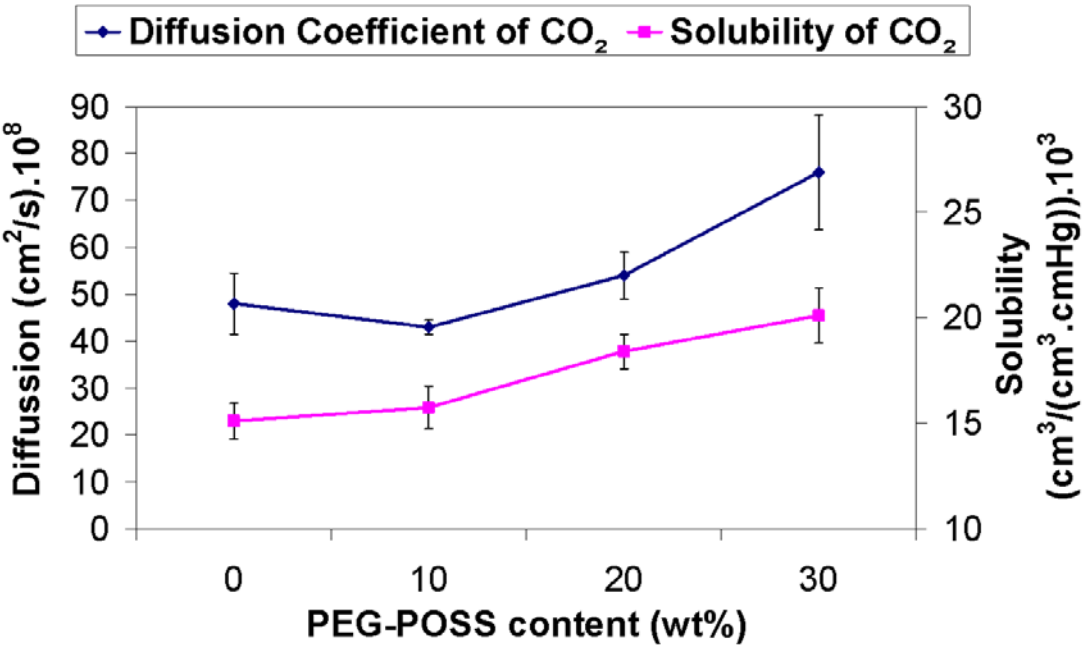
Diffusion Coefficient of CO2
Solubility of CO2
Diffussion (cm2/s).10^8
Solubility (cm3/(cm3.cmHg)).10^3
90
80
70
60
50
40
30
20
10
0
30
25
20
15
10
0
10
20
30
PEG-POSS content (wt%)

Figure 5:

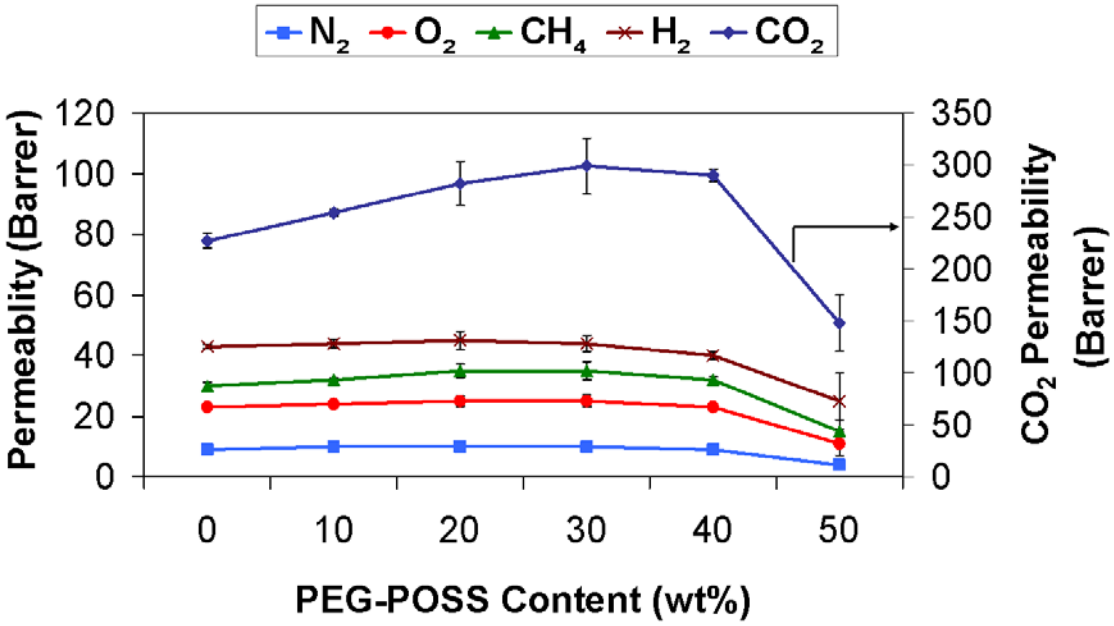
N2
O2
CH4
H2
CO2
Permeablity (Barrer)
120
100
80
60
40
20
0
350
300
250
200
150
100
50
0
CO2 Permeability (Barrer)
0
10
20
30
40
50
PEG-POSS Content (wt%)

Figure 6:

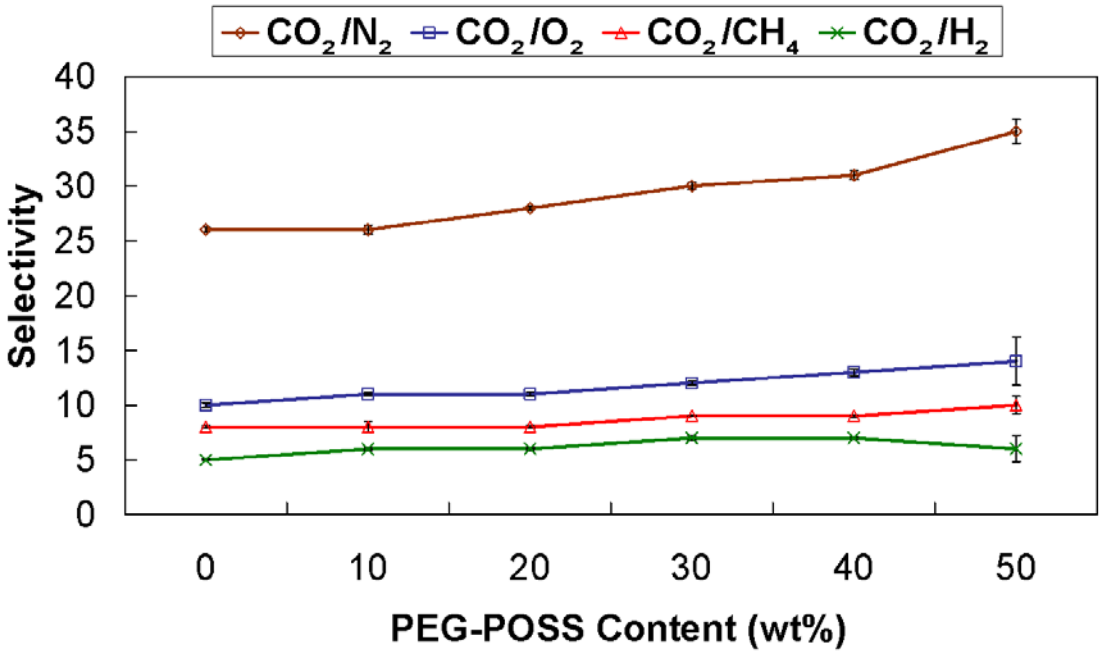
CO2/N2
CO2/O2
CO2/CH4
CO2/H2
Selectivity
40
35
30
25
20
15
10
5
0
0
10
20
30
40
50
PEG-POSS Content (wt%)

Figure 7:

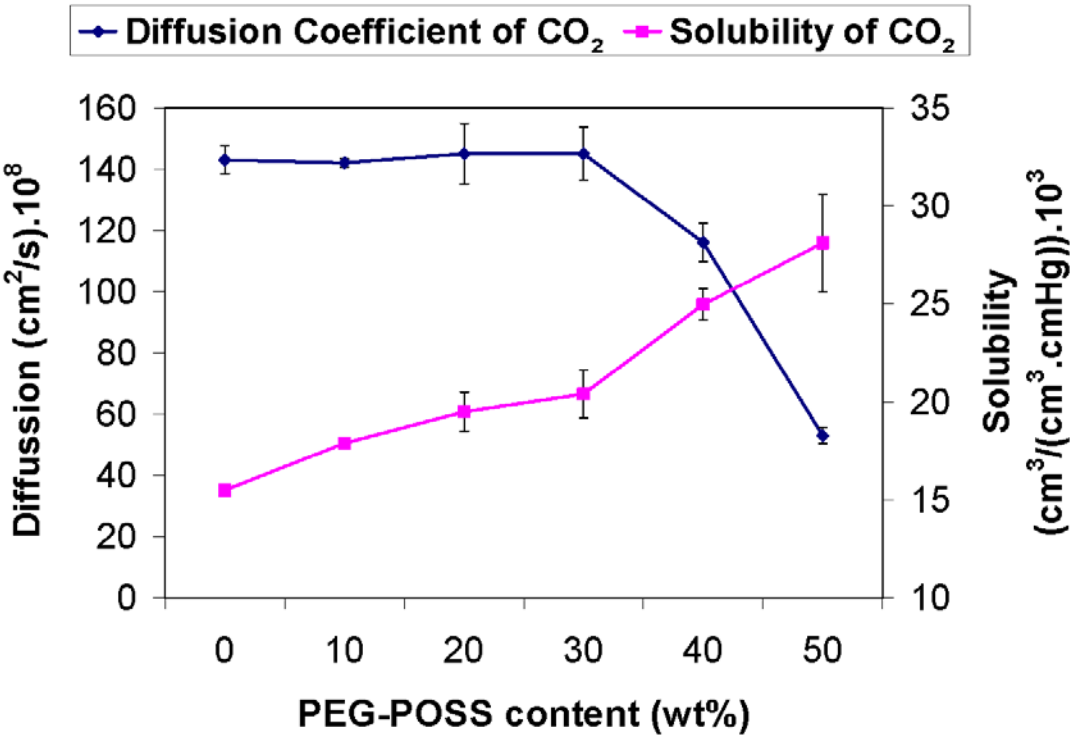
Diffusion Coefficient of CO2
Solubility of CO2
Diffussion (cm2/s).10^8
Solubility (cm3/(cm3.cmHg)).10^3
160
140
120
100
80
60
40
20
0
35
30
25
20
15
10
0
10
20
30
40
50
PEG-POSS content (wt%)

Figure 8:

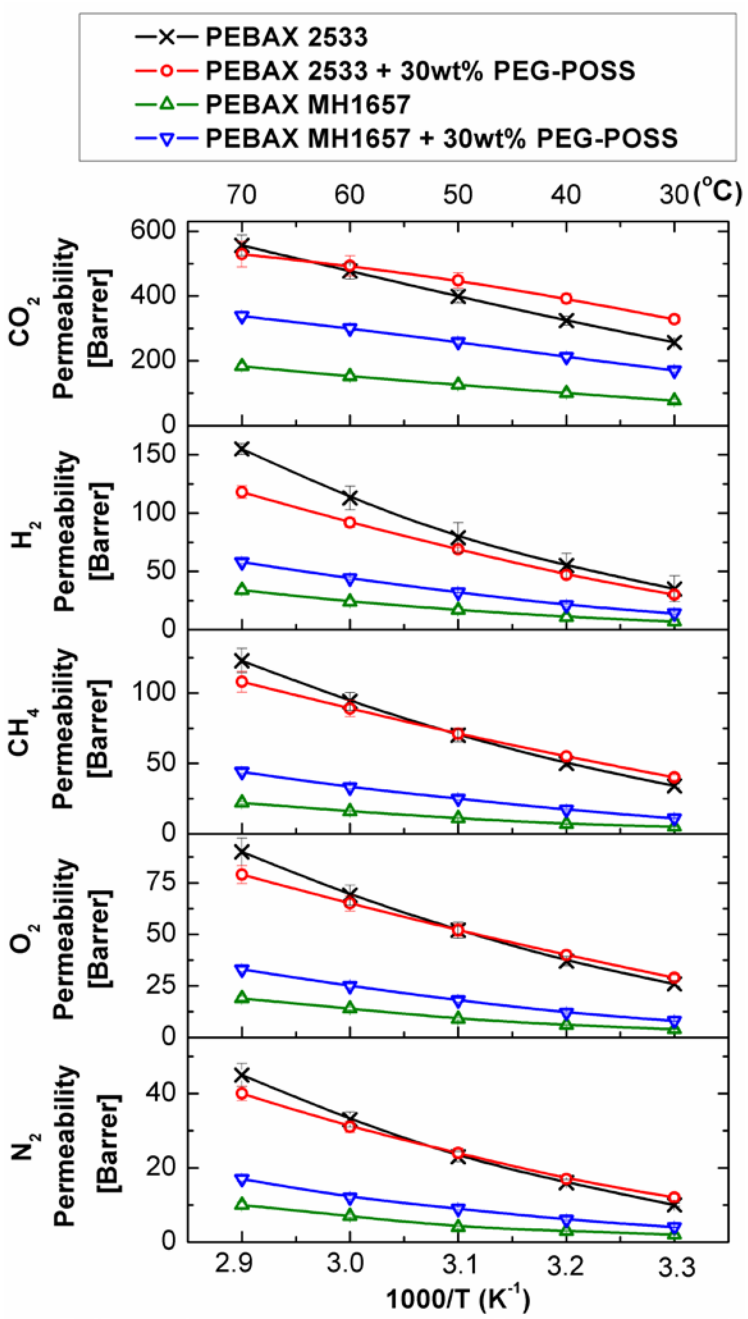
PEBAX 2533
PEBAX 2533 + 30wt% PEG-POSS
PEBAX MH1657
PEBAX MH1657 + 30wt% PEG-POSS
70
60
50
40
30 (°C)
CO2 Permeability [Barrer]
600
400
200
0
H2 Permeability [Barrer]
150
100
50
0
CH4 Permeability [Barrer]
100
50
0
O2 Permeability [Barrer]
75
50
25
0
N2 Permeability [Barrer]
40
20
0
2.9
3.0
3.1
3.2
3.3
1000/T (K-1)

Figure 9:

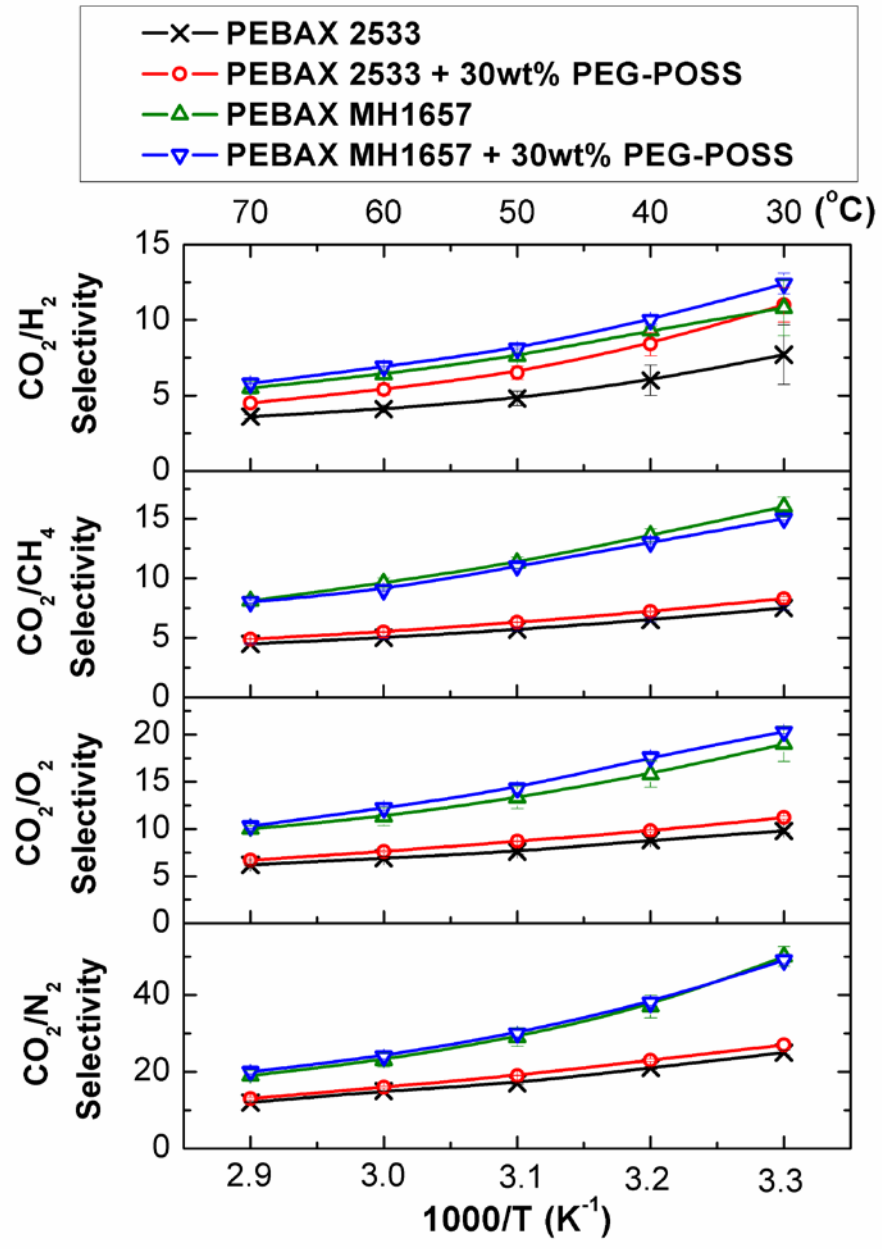
PEBAX 2533
PEBAX 2533 + 30wt% PEG-POSS
PEBAX MH1657
PEBAX MH1657 + 30wt% PEG-POSS
70
60
50
40
30 (°C)
CO2/H2 Selectivity
CO2/CH4 Selectivity
CO2/O2 Selectivity
CO2/N2 Selectivity
0
5
10
15
20
40
2.9
3.0
3.1
3.2
3.3
1000/T (K-1)

Figure 10:

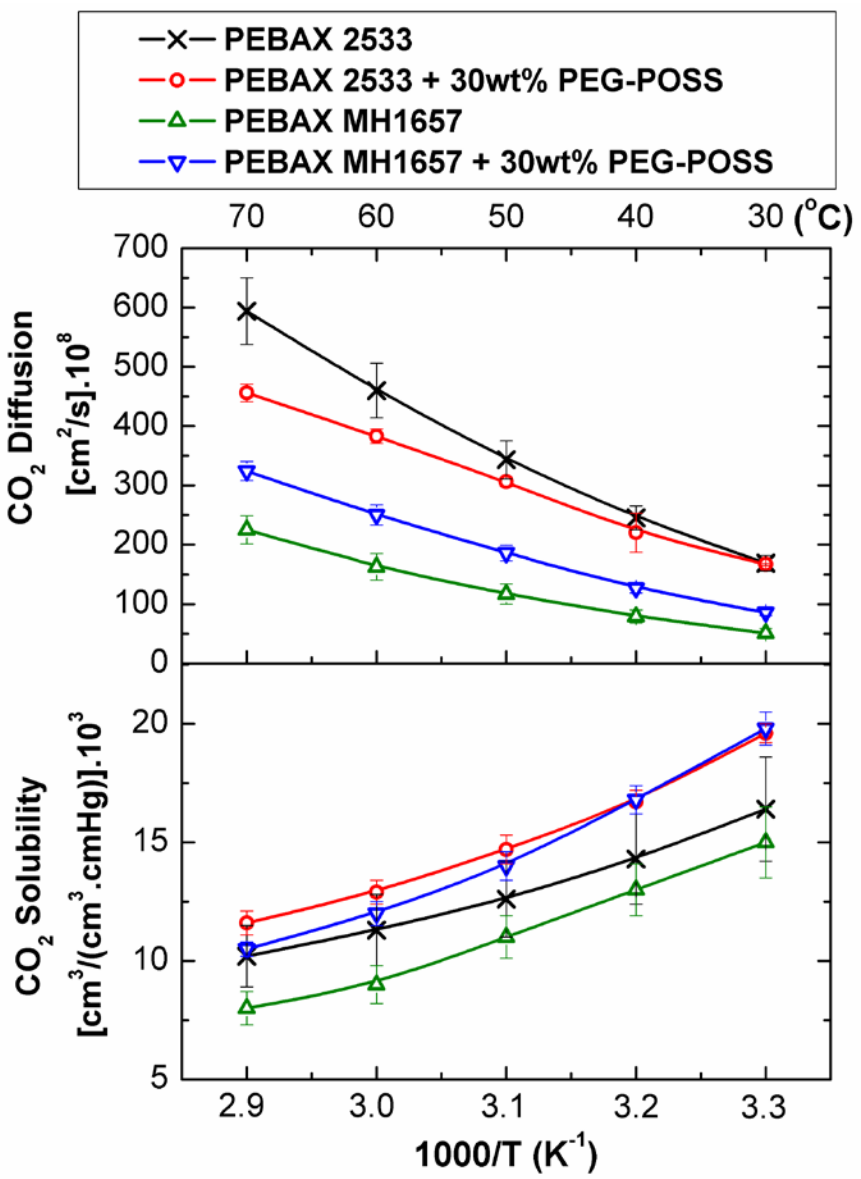
PEBAX 2533
PEBAX 2533 + 30wt% PEG-POSS
PEBAX MH1657
PEBAX MH1657 + 30wt% PEG-POSS
70
60
50
40
30 (°C)
CO2 Diffusion [cm2/s].10^8
700
600
500
400
300
200
100
0
CO2 Solubility [cm3/(cm3.cmHg)].10^3
20
15
10
5
2.9
3.0
3.1
3.2
3.3
1000/T (K-1)

Figure 11:

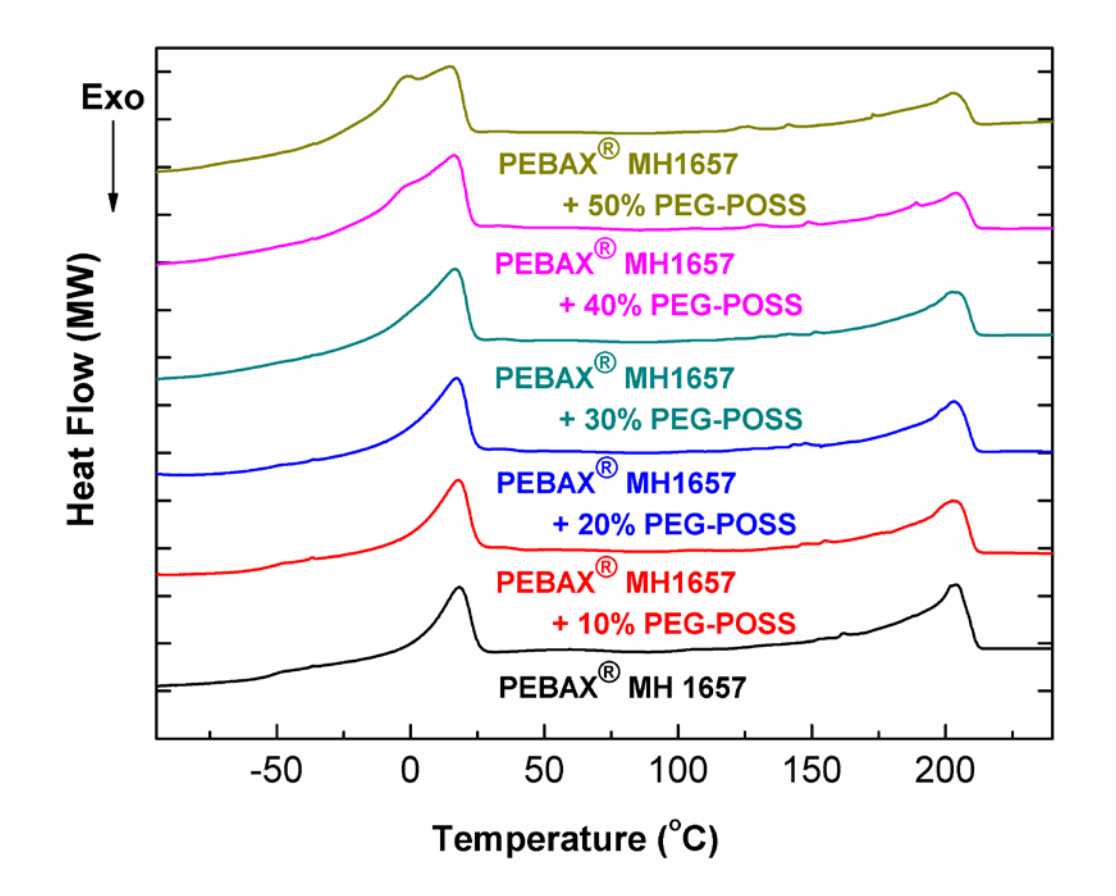
Exo
Heat Flow (MW)
PEBAX® MH1657
+ 50% PEG-POSS
PEBAX® MH1657
+ 40% PEG-POSS
PEBAX® MH1657
+ 30% PEG-POSS
PEBAX® MH1657
+ 20% PEG-POSS
PEBAX® MH1657
+ 10% PEG-POSS
PEBAX® MH 1657
-50
0
50
100
150
200
Temperature (°C)

Figure 12:

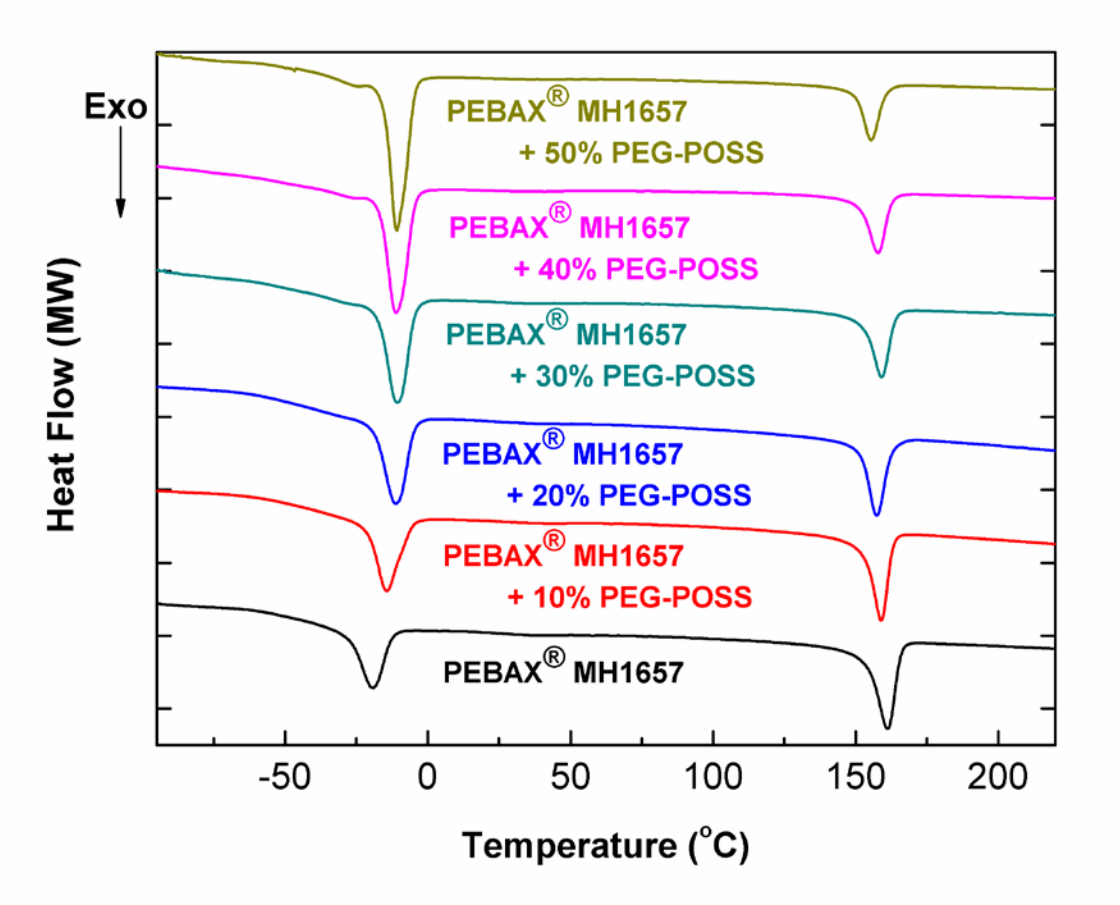
Exo
Heat Flow (MW)
PEBAX® MH1657
+ 50% PEG-POSS
PEBAX® MH1657
+ 40% PEG-POSS
PEBAX® MH1657
+ 30% PEG-POSS
PEBAX® MH1657
+ 20% PEG-POSS
PEBAX® MH1657
+ 10% PEG-POSS
PEBAX® MH1657
-50
0
50
100
150
200
Temperature (°C)

Figure 13:

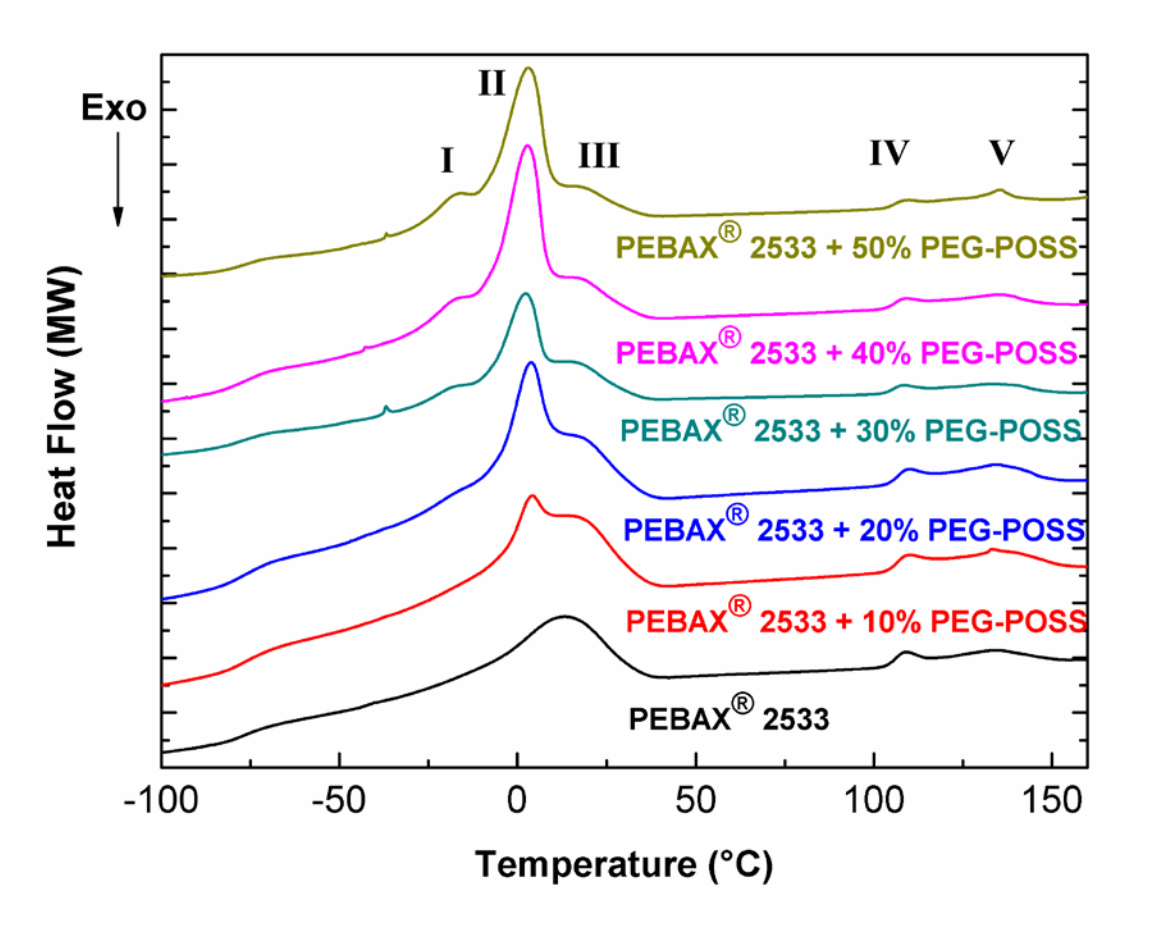
Exo
Heat Flow (MW)
I
II
III
IV
V
PEBAX® 2533 + 50% PEG-POSS
PEBAX® 2533 + 40% PEG-POSS
PEBAX® 2533 + 30% PEG-POSS
PEBAX® 2533 + 20% PEG-POSS
PEBAX® 2533 + 10% PEG-POSS
PEBAX® 2533
-100
-50
0
50
100
150
Temperature (°C)

Figure 14:

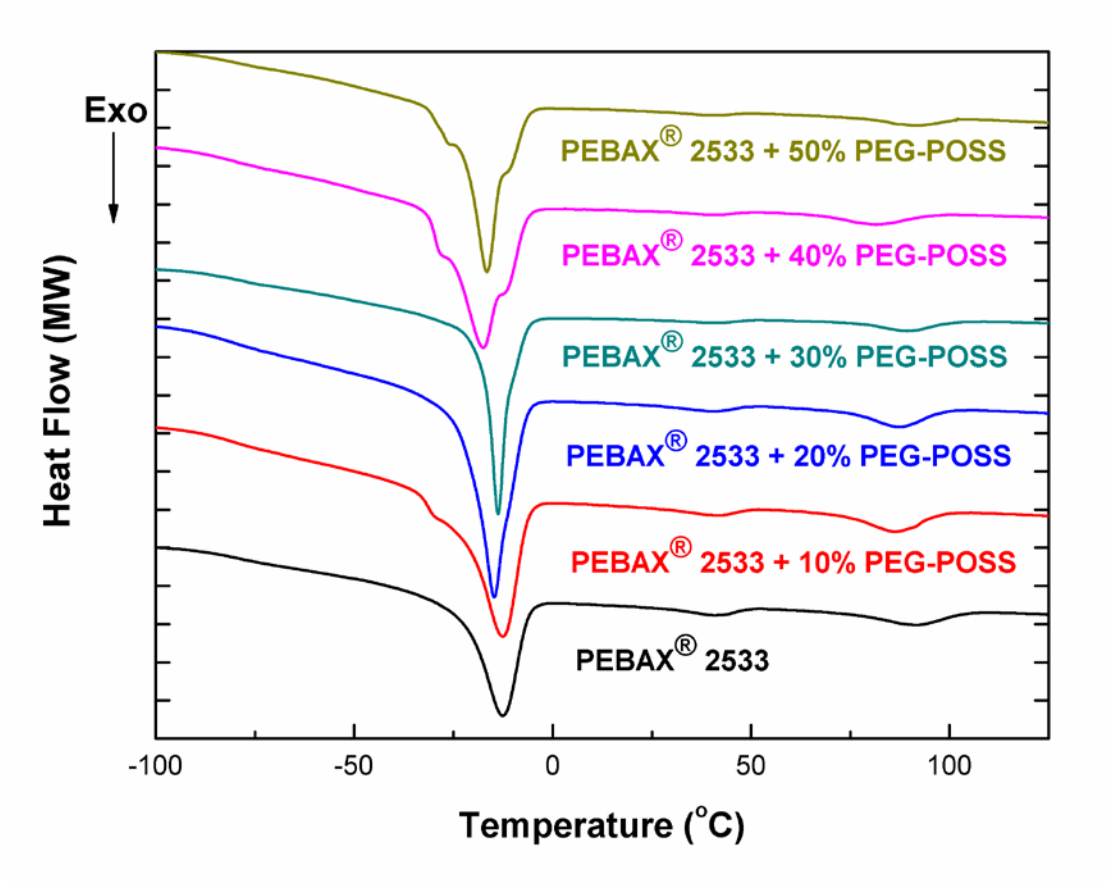
Exo
Heat Flow (MW)
PEBAX® 2533 + 50% PEG-POSS
PEBAX® 2533 + 40% PEG-POSS
PEBAX® 2533 + 30% PEG-POSS
PEBAX® 2533 + 20% PEG-POSS
PEBAX® 2533 + 10% PEG-POSS
PEBAX® 2533
-100
-50
0
50
100
Temperature (°C)

Figure 15:

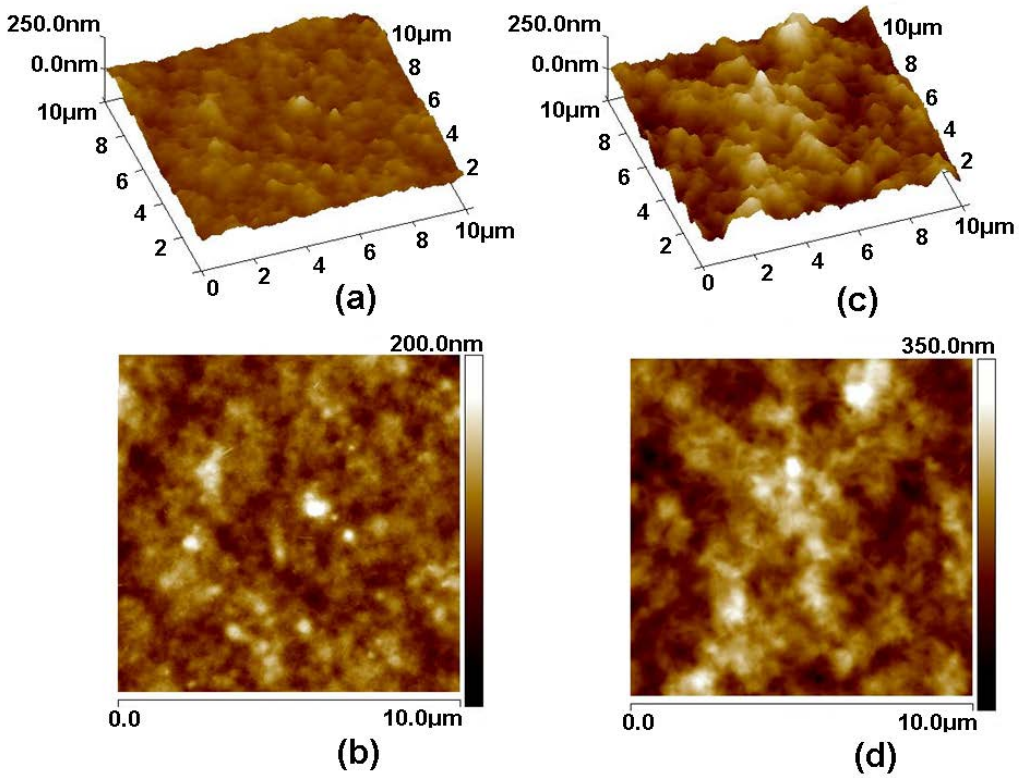
250.0nm
0.0nm
10µm
8
6
4
2
0
2
4
6
8
10µm
(a)
250.0nm
0.0nm
10µm
8
6
4
2
0
2
4
6
8
10µm
(c)
200.0nm
0.0
10.0µm
(b)
350.0nm
0.0
10.0µm
(d)

Figure 16:

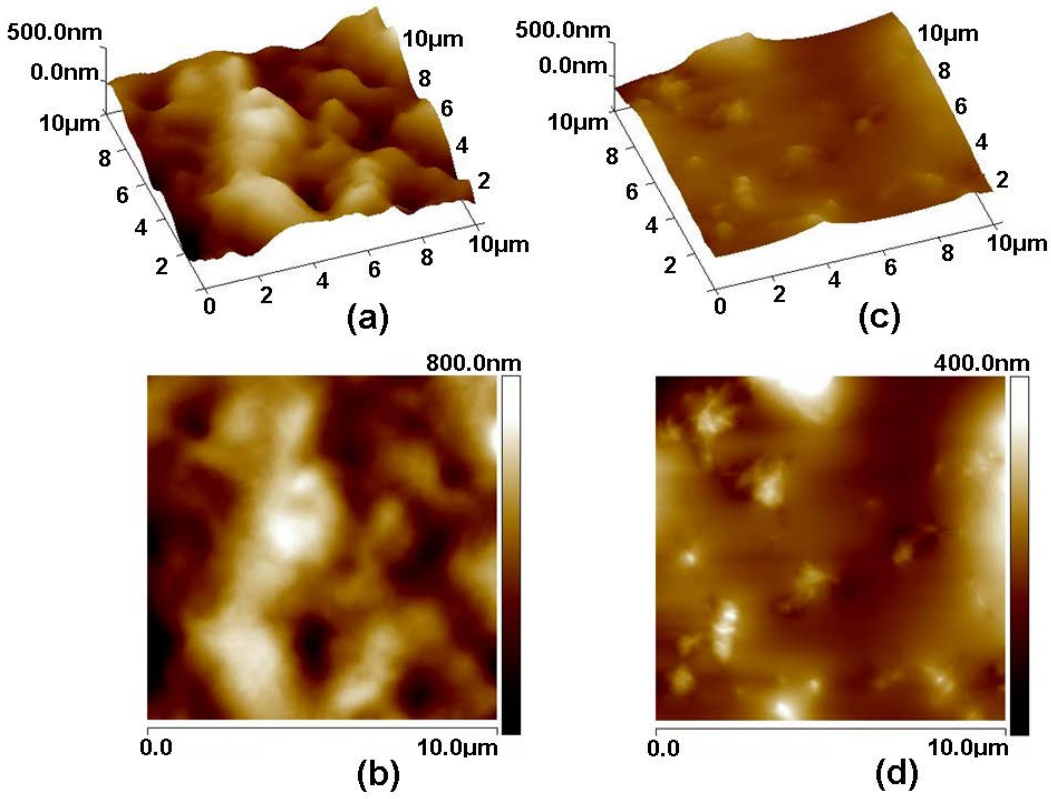
500.0nm
0.0nm
10µm
8
6
4
2
0
2
4
6
8
10µm
(a)
500.0nm
0.0nm
10µm
8
6
4
2
0
2
4
6
8
10µm
(c)
800.0nm
0.0
10.0µm
(b)
400.0nm
0.0
10.0µm
(d)

Figure 17:

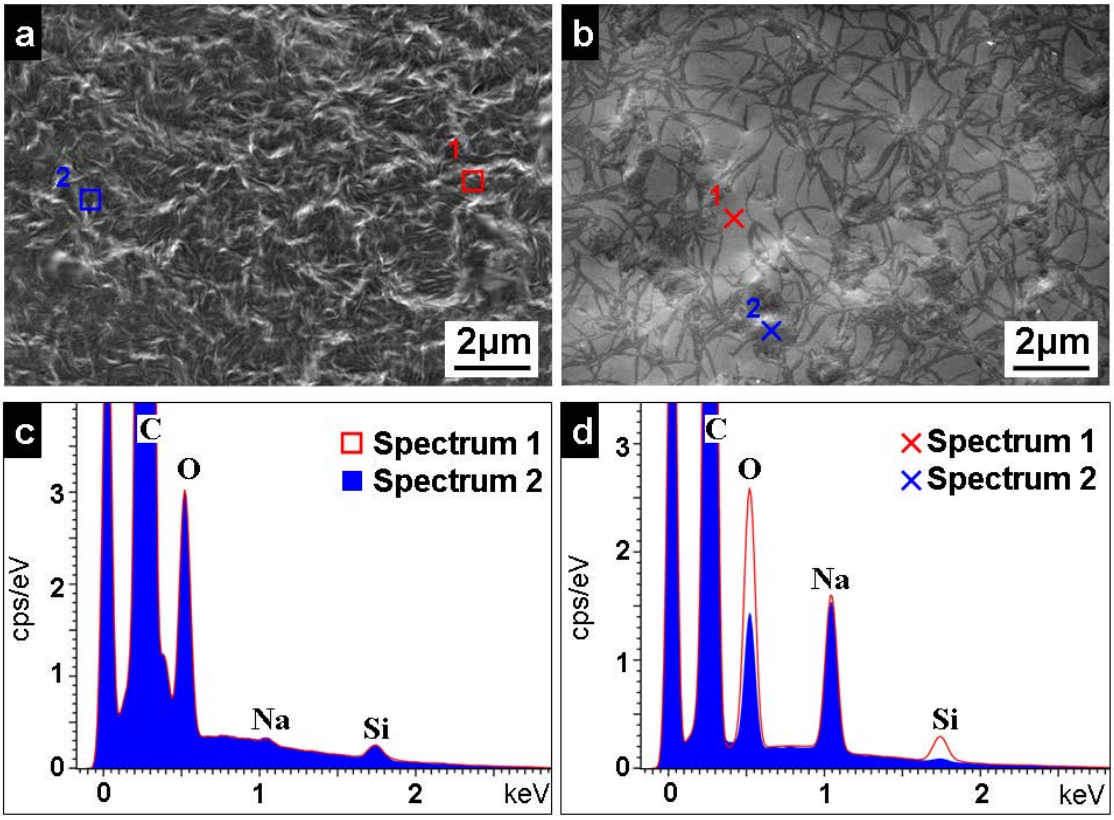
a
1
2
2μm
b
1
2
2μm
c
C
O
Na
Si
Spectrum 1
Spectrum 2
cps/eV
keV
d
C
O
Na
Si
Spectrum 1
Spectrum 2
cps/eV
keV

Figure 18:

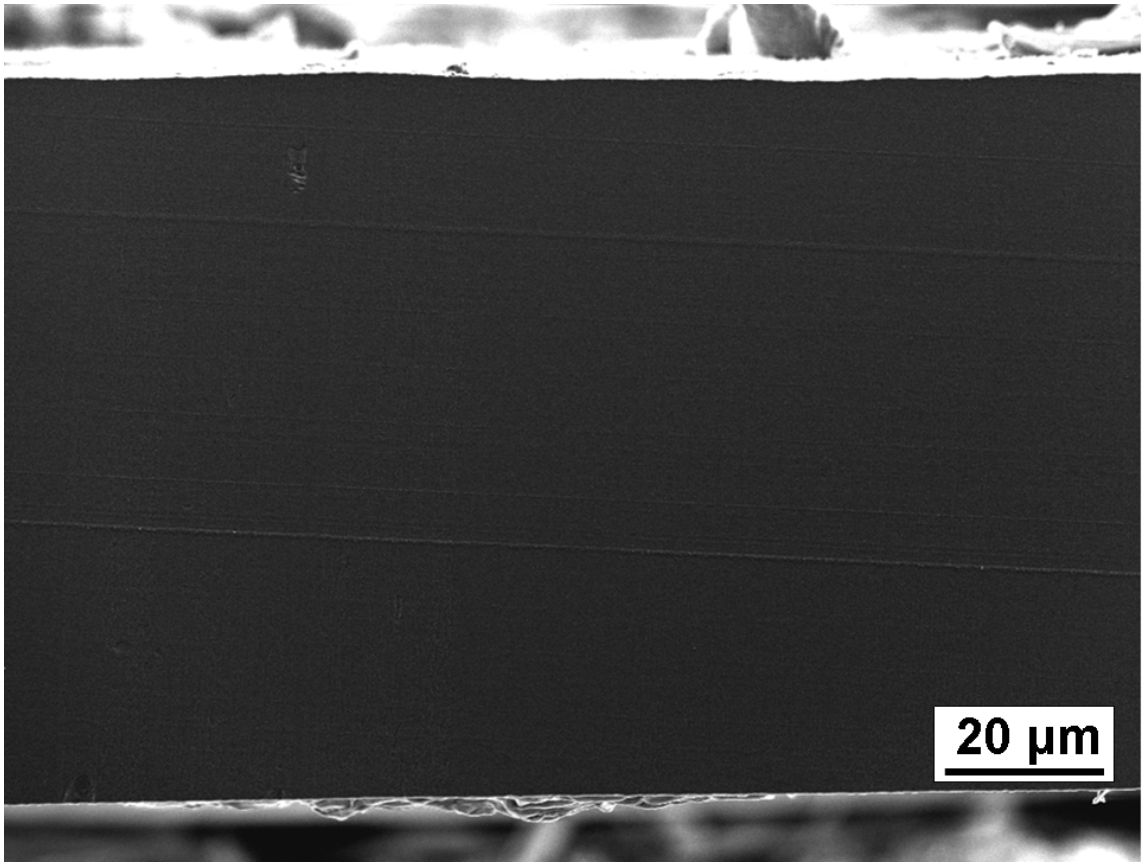

Figure 19:

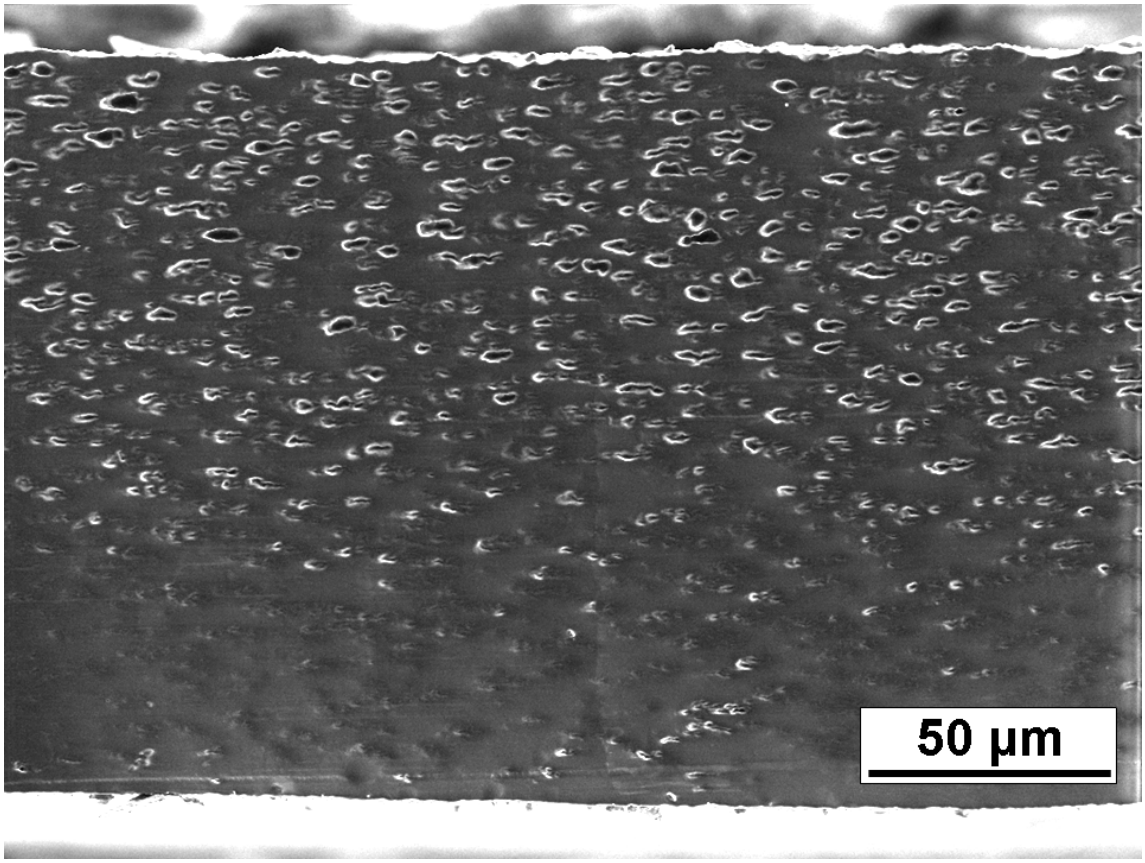

Figure 20:

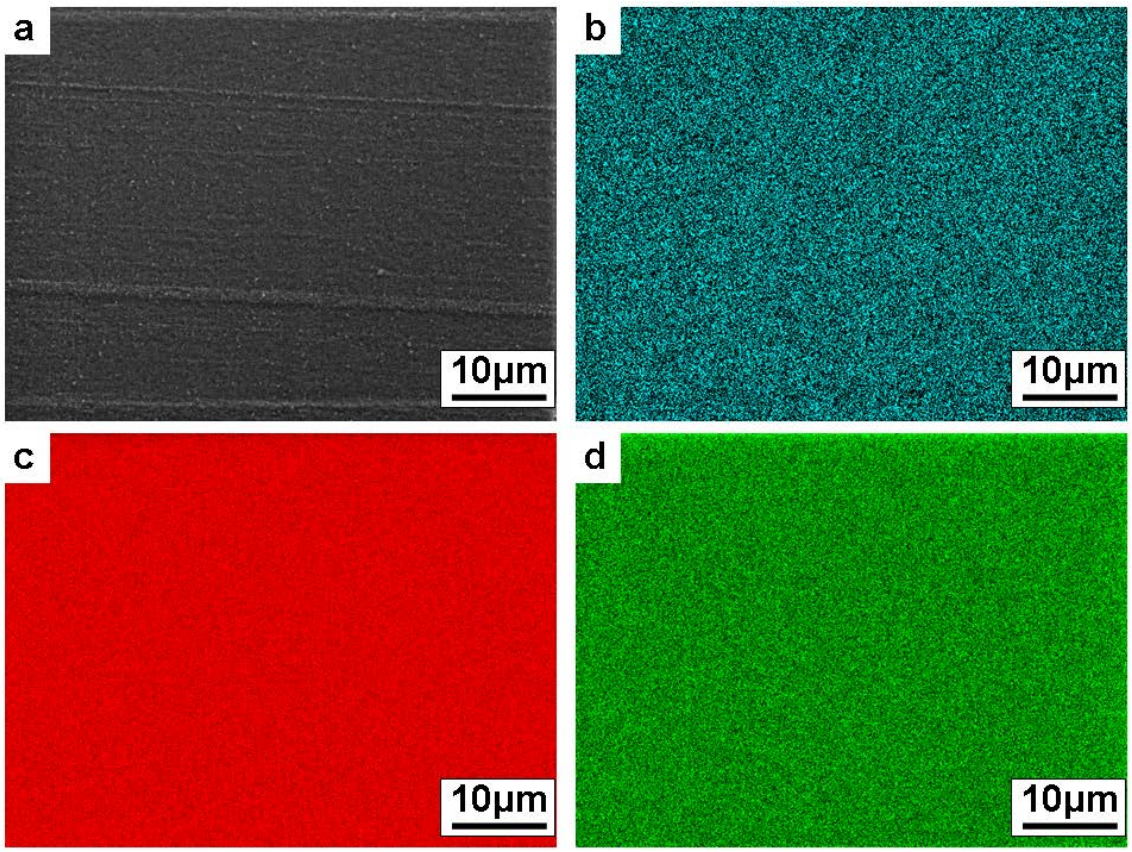

Legend of figures-

Figure 1: Composition of PEG-POSS (a) Structure provided by manufacturer (b) Thermogravimetric analysis.

Figure 2: Single gas permeability as a function of PEG-POSS content in PEBAX® MH1657. Permeability of N_2, O_2, CH_4 and H_2 are plotted on left Y axis and that of CO_2 right Y axis.

Figure 3: CO_2 selectivity over light gases as a function of PEG-POSS content in PEBAX® MH1657.

Figure 4: Diffusion coefficient and solubility of CO_2 as a function of PEG-POSS content in PEBAX® MH1657.

Figure 5: Single gas permeability as a function of PEG-POSS content in PEBAX® 2533. Permeability of N_2, O_2, CH_4 and H_2 are plotted on left Y axis and that of CO_2 right Y axis.

Figure 6: CO_2 selectivity over light gases as a function of PEG-POSS content in PEBAX® 2533.

Figure 7: Diffusion coefficient and solubility of CO_2 as a function of PEG-POSS content in PEBAX® MH1657.

Figure 8: Permeability of gases as a function of temperature of PEBAX® MH1657 and PEBAX® 2533 before and after 30 wt% PEG-POSS incorporation.

Figure 9: CO_2 selectivity over light gases as a function of temperature of PEBAX® MH1657 and PEBAX® 2533 before and after incorporation of 30 wt% PEG-POSS.

Figure 10: Diffusion coefficient and solubility of CO_2 as a function of temperature of PEBAX® MH1657 and PEBAX® 2533 before and after incorporation of 30 wt% PEG-POSS.

Figure 11: DSC thermogram (second heating trace) of PEBAX® MH1657 and its nanocomposites with PEG-POSS.

Figure 12: DSC thermogram (second cooling trace) of PEBAX® MH1657 and its nanocomposites with PEG-POSS.

Figure 13: DSC thermogram (second heating trace) of PEBAX® 2533 and its nanocomposites with PEG-POSS.

Figure 14: DSC thermogram (second cooling trace) of PEBAX® 2533 and its nanocomposites with PEG-POSS.

Figure 15: Surface topography via AFM a) 3D- image of PEBAX® MH1657 c) 3d-image of 30 wt% PEG-POSS incorporated PEBAX® MH1657 b) Height image of PEBAX® MH1657 d) Height image of 30 wt% PEG-POSS incorporated PEBAX® MH1657.

Figure 16: Surface topography via AFM a) 3D- image of PEBAX® 2533 c) 3d-image of 30wt% PEG-POSS incorporated PEBAX® 2533 b) Height image of PEBAX® 2533 d) Height image of 30 wt% PEG-POSS incorporated PEBAX® 2533.

Figure 17: Surface morphology and surface spectra of PEBAX® nanocomposite membranes containing 30 wt% PEG-POSS. a) SEM micrograph of PEBAX® MH1657 nanocomposite membrane; b) SEM micrograph of PEBAX® 2533 nanocomposite membrane; c) EDS spectra of two areas of PEBAX® MH1657 nanocomposite membrane; d) EDS spectra of two areas of PEBAX® 2533 nanocomposite membrane.

Figure 18: SEM micrograph of the cross section of a PEBAX® MH1657 nanocomposite membrane containing 30 wt% PEG-POSS.

Figure 19: SEM micrograph of the cross section of a PEBAX® 2533 nanocomposite membrane containing 30 wt% PEG-POSS.

Figure 20: Cross section morphology of a PEBAX® MH1657 nanocomposite membrane containing 30 wt% PEG-POSS a) SEM micrograph b) Si element map c) C element map d) O element map

Figure 21: Cross section morphology of a PEBAX® 2533 nanocomposite membrane containing 30 wt% PEG-POSS a) SEM micrograph b) Si element map c) C element map d) O element map.

Legend of tables-

Table 1: Composition of two grades of PEBAX®.

Table 2: E_P, E_D and ΔH_S of PEBAX® MH1657 and PEBAX® 2533 before and after 30 wt% PEG-POSS incorporation.

Table 3: Glass transition temperature of PEBAX® MH1657 and PEBAX® 2533 as a function of PEG-POSS content.

Table 4: Onset, peak and endset temperature of crystallization of polyether domain of PEBAX® MH1657 as a function of PEG-POSS content.

Table 5: Roughness parameters of PEBAX® MH1657 and PEBAX® MH1657 with 30 wt% PEG-POSS .

Table 6: Roughness parameters of PEBAX® 2533 and PEBAX® 2533 with 30 wt% PEG-POSS.